Investigating the rapid activation of the Futile Creatine Cycle via genetic manipulation

Zafir Kaiser
Department of Biochemistry
McGill University, Montréal
December 2024

A thesis submitted to McGill University in partial fulfillment of the requirements of the degree of Master's of Science

TABLE OF CONTENTS

ABSTRACT

Brown adipose tissue (BAT) generates heat from macronutrient-derived energy in a process called non-shivering thermogenesis. Futile substrate cycles that consume ATP without performing work are thermogenic systems with the potential to combat obesity and metabolic diseases. The futile creatine cycle (FCC) contributes to adipocyte thermogenesis by triggering ATP turnover through the coordinated activities of creatine kinase B (CKB) and tissue non-specific alkaline phosphatase (TNAP). We recently identified glycerol as an allosteric activator of TNAP that resultantly amplifies FCC activity. When glycerol accumulates within brown adipocytes, it is exported out by aquaglyceroporins. In this present study, we set out to ascertain whether genetic manipulation of glycerol transport serves as a mode of facultative FCC activation, hypothesizing that preventing glycerol efflux would trap glycerol intracellularly and present an opportunity to rapidly activate the FCC through enhanced TNAP activity. By mining ribosome profiling data, we validated aquaporin 7 (Aqp7) as the most abundant glycerol transporter in BAT. In immortalized brown adipocytes, knockdown of Aqp7 resulted in decreased glycerol efflux concomitant with increased intracellular glycerol following noradrenaline-stimulated lipolysis. To translate this successful 'trapping' to FCC activity, we performed a series of *in vitro* and *ex vivo* respirometry experiments. Unexpectedly, intracellular glycerol accumulation decreased noradrenaline-stimulated respiration in both immortalized and mature brown adipocytes. Moreover, adipocyte-specific knockdown of Aqp7 *in vivo* resulted in decreased whole-body energy expenditure. While these findings shed light on the regulatory role of glycerol in thermogenesis, it is unclear whether excess intracellular glycerol decreases respiratory capacity in brown adipocytes due to metabolic defects or BAT whitening. Therefore, further investigation is required to establish the suitability of Aqp7 in BAT as a target for FCC hyperactivation.

RÉSUMÉ

Le tissu adipeux brun (TAB) génère de la chaleur à partir de l'énergie dérivée des macronutriments provenant de la thermogenèse sans frisson. Les cycles futiles qui consomment l'ATP sans effectuer de travail sont des systèmes thermogéniques qui peuvent être utiles dans la lutte contre l'obésité et les maladies métaboliques. Le cycle futile de la créatine (CFC) contribue à la thermogenèse adipocytaire en déclenchant le renouvellement de l'ATP grâce aux activités coordonnées de la créatine kinase B (CKB) et de la phosphatase alcaline non spécifique des tissus (PANT). Nous avons récemment identifié le glycérol comme un activateur allostérique de la PANT qui amplifie l'activité de la CFC. Le glycérol accumulé dans les adipocytes bruns est exporté par les aquaglycéroporines. Dans cette étude, nous avons cherché à déterminer si la manipulation génétique du transport du glycérol peut déclencher l'activation facultative du CFC. Nous avons avancé l'hypothèse que le blocage de l'efflux du glycérol piégerait le glycérol à l'intérieur des cellules, ce qui permettrait l'activation du CFC grâce à l'augmentation de l'activité catalytique de la PANT. En exploitant les données de profilage des ribosomes, nous avons validé que l'aquaporine 7 (Aqp7) est le transporteur du glycérol le plus abondant dans les TAB. Dans les adipocytes bruns immortalisés, le knockdown de l'Aqp7 a diminué l'efflux du glycérol et a simultanément augmenté la concentration du glycérol intracellulaire suivant une lipolyse stimulée par la noradrénaline. Pour lier l'accumulation du glycérol intracellulaire à l'activité du CFC, nous avons réalisé une série d'expériences de respirométrie *in vitro* et *ex vivo*. Contre toute attente, l'accumulation du glycérol intracellulaire a diminué la respiration stimulée par la noradrénaline dans les adipocytes bruns immortalisés ainsi que dans les adipocytes bruns matures. En outre, le knockdown spécifique de l'Aqp7 dans les adipocytes *in vivo* a entraîné une diminution de la dépense énergétique du corps entier. Bien que ces résultats mettent en lumière le rôle du glycérol dans la régulation de la thermogenèse, il n'est pas clair si un excès de glycérol intracellulaire diminue la capacité respiratoire en raison de défauts métaboliques ou du blanchiment des BAT. Par consequent d'autres études sont nécessaires pour déterminer la pertinence de l'Aqp7 dans les TAB comme une cible pour l'hyperactivation de la CFC.

ACKNOWLEDGEMENTS

To begin, I thank my supervisor, Dr. Lawrence Kazak, for taking a chance on me to join his lab, providing me with the freedom to explore an array of projects, and for continued support over the years. I am immensely grateful for my lab mates with whom I shared my Master's degree experience: Jakub Bunk, Janane Rahbani, Faiz Hussain, Anna Roesler, Chris Dykstra, Bozena Samborska and many more. Thank you to the members of my research advisory committee, Dr. John Orlowski and Dr. Thomas Duchaine, for your comments and guidance. I want to thank my past mentors from my undergraduate years at McGill for providing a platform to begin my research journey, perspective on the field, and unwavering support throughout the years: Dr. Alexandre Orthwein, Dr. Mary Stevenson, and Dr. Steven Findlay. Lastly, thank you to my friends and family who supported me and believed in me unconditionally. Funding was provided by the Canada Graduate Scholarships Master's Program from The Natural Sciences and Engineering Research Council of Canada (NSERC).

CONTRIBUTION OF AUTHORS

I, Zafir Kaiser (ZK), performed all the work presented in this thesis except for the following: 1) Samples for non-wild-type *in vivo* cold exposure experiments were provided by Janane Rahbani (JR) from cDNA library [82], on which ZK performed RT-qPCR; 2) Avertin injections and indirect calorimetry experiments were performed and analyzed with assistance from Jakub Bunk (JB) and Faiz Hussain (FH) using virus prepared by ZK.

CONFLICT OF INTEREST

I, ZK, declare I have no conflict of interest.

APPENDIX: LIST OF FIGURES AND TABLES

Table 1.0 – List of Abbreviations

Abbreviation	Description
AAV	Adeno-associated virus
AC	Adenyl cyclase
ACC	Acetyl-CoA carboxylase
ADP	Adenosine diphosphate
AQP	Aquaporin
AR	Adrenergic receptor
ATGL	Adipose triglyceride lipase
ATP	Adenosine triphosphate
BAT	Brown adipose tissue
BCAA	Branch-chain amino acid
BMI	Body mass index
BMR	Basal metabolic rate
BSA	Bovine serum albumin
cAMP	Cyclic adenosine monophosphate
CK	Creatine kinase
CKB	Creatine kinase brain-type
Cr	Creatine
CREB	cAMP-response element binding protein
DGAT	Diglyceride acyltransferase
DHAP	Dihydroxyacetone phosphate
DIT	Diet-induced thermogenesis
DMEM	Dulbecco's Modified Eagle's Medium
DNL	*de novo* lipogenesis
DNP	2,4-Dinitrophenol
EBF	Early B cell factor
EE	Energy expenditure
EI	Energy intake
EM	Electron-microscopy
ETC	Electron transport chain
eWAT	Epididymal white adipose tissue
$FADH_2$	Flavin adenine dinucleotide
FASN	Fatty acid synthase
FBS	Fetal bovine serum
FCC	Futile creatine cycle
FDG	Fluorodeoxyglucose
FFA	Free fatty acid
G3P	Glycerol-3-phosphate
GATM	Glycine amidinotransferase
GDP	Guanosine diphosphate
GK	Glycerol kinase
GPAT	Glycerol-3-phosphate acyltransferases
GPCR	G protein-coupled receptors

GTP	Guanosine triphosphate
HSL	Hormone sensitive lipase
IBMX	3-Isobutyl-1-methylxanthine
IP_3	Inositol trisphosphate
iWAT	Inguinal white adipose tissue
KD	Knockdown
KO	Knockout
KRBMB	Krebs-Ringer Bicarbonate Buffer
LCFA	Long-chain fatty acid
LD	Lipid droplet
LPL	Lipoprotein lipase
MGL	Monoglyceride lipase
MHO	Metabolically healthy obesity
MUHO	Metabolically unhealthy obesity
NA	Noradrenaline
NADH	Nicotinamide adenine dinucleotide
NST	Non-shivering thermogenesis
OCR	Oxygen consumption rate
P/S	Penicillin and streptomycin
PBS	Phosphate-buffered saline
PCr	Phosphocreatine
PEG	Polyethylene glycol
PET-CT	Positron emission tomography-computed tomography scan
Pgc1α	Peroxisome proliferator-activated receptor gamma coactivator 1-alpha
PIP_2	Phosphatidylinositol 4,5-bisphosphate
PKA	Protein kinase A
PKC	Protein kinase C
PLC	Phospholipase C
PPAR	Peroxisome proliferator-activated receptor
PTM	Post-translational modification
PVDF	Polyvinylidene difluoride
RBC	Red blood cell
sgRNA	Single guide RNA
shRNA	Short-hairpin RNA
siRNA	Small interfering RNA
SLC6A8	Solute carrier family 6 protein 8
SVF	Stromal vascular fraction
TAG	Triacylglycerol
TBS-T	Tris-buffered saline with Tween
TN	Thermoneutrality
TNAP	Tissue-nonspecific alkaline phosphatase
TPI	Triose phosphate isomerase
UCP1	Uncoupling protein 1
WAT	White adipose tissue
WT	Wild type

LITERATURE REVIEW

Chapter 1: Obesity

1.1 Pathogenesis

Obesity arises when energy intake (EI) chronically exceeds energy expenditure (EE). EI is derived from the chemical energy stored in dietary macrocomponents, which are digested to provide daily EE requirements dependent on basal metabolic rate (BMR) and physical activity levels. A positive energy balance results in the eventual storage of excess EI as triacylglycerols in adipose tissue. Thus, prolonged positive energy balance increases adiposity and excessive weight gain. While energy imbalance is the primary trigger behind the complexity of obesity, it makes way for misguided social stereotypes and stigma targeting obese individuals – incorrectly labelled as lazy or lacking self-discipline. Furthermore, it reinforces a false dichotomy that being overweight is a choice. Many studies highlight that obesity is a multifactorial disease that stems from various factors: behavioural, genetic, hormonal, socioeconomic, and environmental [12]. Altogether, the unique interaction of these factors creates the chronic net positive energy balance that leads to obesity pathogenesis.

1.2 Prevalence and Significance

Around 1830, Adolphe Quetelet developed the Body Mass Index (BMI) to classify individuals into one of four categories: underweight, healthy, overweight, and obese. BMI is a function of an individual's mass (measured in kilograms, kg) divided by their height (measured in metres, m) squared. The World Health Organization schema classifies a BMI between 25 & 30 kg/m^2 as overweight and a BMI greater than 30 kg/m^2 as obese [13]. The index remains widely used to measure obesity rates despite some limitations. For instance, BMI does not consider age, sex, muscle mass, body fat percentage, bone density, or health history. Therefore, it is not the perfect diagnostic determinant for obesity, but it is an excellent tool for detecting macroscale obesity rates.

Since 1990, global adult and adolescent obesity rates have more than doubled and quadrupled, respectively [14, 15]. This is particularly alarming as over 75% of obese children go on to become obese adults [16]. The pervasiveness of overweight and obese individuals increases in both developed and developing countries – posing major global health concerns. On the one hand, in developed nations such as Canada, widespread consumption of processed foods and physical activity patterns transitioning towards sedentary lifestyles have compounded the discrepancy between increasing EI and decreasing EE. Currently, more than 1 in 4 adult Canadians live with obesity [17]. On the other hand, developing nations face shortages of affordable healthy foods. Roughly three billion people cannot afford a healthy diet and resort to energy-dense and nutrient-poor diets due to this heightened cost disparity [18]. Obesity also significantly increases the risk of other health conditions, such as cardiovascular diseases, type 2 diabetes, and some cancers [12]. Moreover, complications of obesity are not restricted to physical health concerns, as psychiatric conditions are linked to excess weight. Associated comorbidities tied to obesity place a significant economic burden by increasing healthcare system costs while decreasing the value of economic output due to premature deaths and disabilities of working citizens. The financial burden of obesity in Canada ranges from $4.6 billion to $7.1 billion annually [17]. Obesity is viewed as a more significant global health risk than hunger due to recent paradigm shifts.

1.3 Treatment Options and Therapeutic Targets

Obesity treatment strives to achieve a ‘healthy’ weight (BMI 18.5-24.9 kg/m^2) by decreasing EI or increasing EE to improve overall health and lower the risk of developing associated co-morbidities. However, simply losing the excess weight is not adequate, as more than 80% of obese individuals who lose weight will regain it [19]. For instance, consider liposuction procedures which remove excess adipose tissue without improving metabolic parameters such as the underlying insulin resistance and risk factors for cardiovascular disease [20]. Without correcting the fundamental energy imbalance problem, the fat mass redeposits at the site of excision or other depots within a year [20].

Therefore, the sustainability and maintenance of treatments are integral to a long-term solution.

Lifestyle changes in the form of increasing physical activity and reducing calorie intake are paramount to counteract obesity. Despite this understanding, adherence is low and, in some cases, an oversimplification of the aforementioned external factors that contribute to obesity [12]. Thus, while lifestyle modifications are a crucial first step toward weight loss, they are often complemented by pharmaceutical and surgical interventions. Anti-obesity pharmaceuticals such as Bupropion/Naltrexone and Semaglutide, approved by Health Canada, respectively, aim to reduce EI through appetite suppression via neurohormonal pathways and impairment of intestinal fat absorption [21]. However, variable efficacy and side effects such as nausea and constipation are noteworthy drawbacks. Bariatric surgeries aim to reduce EI by decreasing stomach volume to promote satiety or limit absorbed calories and nutrients, but nutritional and vitamin deficiencies may arise from malabsorption [22]. While most current treatments focus on decreasing EI, increasing EE provides another avenue to combat obesity.

Intriguingly, activating specific metabolic pathways within the adipose tissue pool can significantly elevate EE to establish a negative energy balance and ameliorate obesity [2,3,4,7,8]. Conventionally, adipose tissue has been classified as white adipose tissue (WAT) and brown adipose tissue (BAT). Moreover, the mammalian adipose tissue pool is comprised of developmentally and functionally distinct subsets of adipocytes. Despite this, the entire organ is commonly viewed as undesirable and cast under the shadow of obesity and its comorbidities. Such stigmatization distracts from a fascinating aspect of adipose tissue biology in metabolic health and its anti-obesogenic potential.

Chapter 2 & 3: Adipose Tissue

2.1 White Adipose Tissue

Adipose tissue is a specialized connective tissue within a mesh-like extracellular matrix. All depots are highly heterogeneous and consist of adipocytes, pre-adipocytes, fibroblasts, endothelial cells, stromal cells, and immune cells [23]. WAT specifically can

constitute up to 25% of body weight in healthy individuals and is the long-term storage site of excess calories consumed as energy-dense triacylglycerol (TAGs). TAG stores can then be accessed during periods of low-calorie intake. One TAG unit consists of three fatty acids bonded via ester bonds to a glycerol backbone. According to the Atwater general factor system, the oxidation of fats provides 37 kJ/g (9.0 kcal/g) of energy compared to 17 kJ/g (4.0 kcal/g) for carbohydrates and proteins [24]. This significant increase in energy density is due to more reduced carbon atoms and higher electron-density fatty acids. However, fat's high energy density presents a double-edged sword. Although WAT yields evolutionary advantages in periods of starvation, this property of high-fat foods causes overconsumption and rising obesity rates.

In addition to energy storage, WAT cushions vital organs, insulates the body, and serves as an endocrine gland influencing energy metabolism by secreting paracrine factors. Associated hormones, called adipokines, include leptin and ghrelin, which regulate satiety and hunger, respectively. WAT is well-distributed throughout the body and can be categorized as inguinal (subcutaneous) and epididymal (visceral), where the latter depot is associated with metabolic diseases [25]. Inguinal WAT (iWAT) is found within the hypodermis, while epididymal WAT (eWAT) accumulates in the abdominal cavity around vital organs [26]. Moreover, white adipocytes are the most abundant cell type in WAT, comprising 35–75% of all cells. Pax7-/Myf5- progenitors of multipotent mesenchymal stem cell lineage give rise to white preadipocytes, which differentiate into mature white adipocytes [27,28]. White adipocytes are characterized by a large unilocular central lipid droplet (LD) that occupies over 90% of the cell volume, attributing to their spherical morphology, and few elongated organelles (i.e. mitochondria) pushed to the cell’s periphery [27]. LDs store TAGs with other neutral lipids surrounded by a phospholipid monolayer and more than 200 LD-associated proteins [29]. LDs were long thought of as inert stores of lipids, but they are now recognized as highly dynamic organelles. Importantly, WAT is highly responsive to changes in energy levels, from energy surplus (i.e. postprandial state) to energy deprivation (i.e. postabsorptive state).

2.2 White Adipose Tissue Expansion, Contraction, and Remodeling

During overnutrition, WAT sequesters excess macronutrient-derived energy to expand by increasing adipocyte size (hypertrophy) and quantity (hyperplasia) [30]. Hypertrophy begins with TAG synthesis to fill LDs in insulin-sensitive white adipocytes. Metabolic substrates for TAGs are derived from two primary sources. The predominant source is from excess dietary lipids found in circulating lipoproteins. Exogeneous TAGs are hydrolyzed by lipoprotein lipase (LPL) and released into circulation as free fatty acids (FFAs), which non-covalently bind serum albumin and travel to WAT depots [30]. Alternatively, white adipocytes can undergo *de novo* lipogenesis (DNL) using acetyl-CoA derived from excess nonlipid precursors such as carbohydrates, amino acids, and metabolites such as lactate and glycerol [31]. More specifically, cytosolic acetyl-CoA carboxylase (ACC) elongates a fatty acid carbon chain to malonyl-CoA using a series of acetyl-CoA to ultimately form 16-carbon palmitate, a precursor for several fatty acids via fatty acid synthase (FASN). However, endogenous substrates used for DNL account for <2% of adipose TAG content [31]. In the endoplasmic reticulum, exogenous and endogenous FFAs undergo esterification with glycerol for storage in LDs. Briefly, glycerol-3-phosphate acyltransferase (GPAT) catalyzes the rate-limiting for TAG biosynthesis, and two acyl-CoA diacylglycerol acyltransferase (DGAT) enzymes determine the flux of FFAs into TAGs [32]. Hypertrophy continues until a critical threshold of ~0.7–0.8 μg per adipocyte after which additional anabolic stress cannot be housed [32]. Arrival at this juncture stresses adipocytes and triggers a downstream inflammatory response [30]. When the unilocular LD cannot expand further, adipokines signal transition to hyperplasia and induce the proliferation and differentiation of preadipocytes [33]. Overall, both hypertrophy and hyperplasia tightly regulate adipocyte count and turnover rate, which have been shown to be fixed early in life [34].

Healthy WAT expansion is achieved by maximizing adipogenesis and insulin sensitivity while minimizing adipocyte volume and inflammation [30]. When hyperplasia prevails over hypertrophy, WAT expansion protects against many of the adverse metabolic consequences of obesity. This is evident in metabolically healthy obesity (MHO), where individuals primarily accumulate fat in iWAT depots. MHO is not accompanied by extensive insulin resistance, adipose tissue and systemic inflammation. In contrast to MHO, another subgroup is labelled as metabolically unhealthy obesity

(MUHO). MUHO individuals have limited iWAT storage capacity and thus default to eWAT [35]. After prolonged positive energy balance, hyperplasia and hypertrophy become overwhelmed. Fat then accrues in ectopic tissues such as the liver, skeletal muscle, and heart – known as lipotoxicity [36]. These changes increase inflammation and hypertrophy contaminant with decreased adipogenesis and insulin sensitivity. WAT is dysfunctional during unhealthy expansion and cycles between hypertrophy, followed by necrosis & apoptosis, before the appearance of new adipocytes [37].

Under fasted or staving conditions, metabolism transitions to a catabolic postabsorptive state. β-oxidation counteracts fatty acid synthesis and contributes proportionately more to EE than carbohydrate oxidation because of greater lipid availability as glucose becomes limiting [38]. Stored TAGs undergo rapid hydrolysis via three major enzymes – accounting for >90% of adipocyte lipolysis [39]. The initial cleavage of TAGs to diacylglycerols is performed by adipose triglyceride lipase (ATGL) [10]. Next, hormone-sensitive lipase (HSL) hydrolyzes diacylglycerols, and monoglyceride lipase (MGL) completes the final de-esterification to liberate glycerol and FFAs [40]. Bulk glycerol is shuttled to the liver, where it is metabolized to glycolysis intermediate, glyceraldehyde 3-phosphate [41]. FFAs are transported to tissues with high energy demand, where they undergo β-oxidation in the mitochondrial matrix, which produces acetyl-CoA and high-energy electron carriers for EE requirements.

Adipocytes are notoriously difficult to lose after they are gained. While significant weight loss is associated with reduced adipocyte volume, the overall adipocyte number remains steady [42]. This is a major hurdle obese individuals face on their path to a healthy BMI. Studies of obese individuals after weight loss show that their adipose tissue hypercellularity is associated with leptin deficiency, which likely increases appetite and lowers EE [43]. These factors promote lipid accumulation in adipocytes and weight gain towards the status before weight loss. Therefore, tight regulation of adipocyte number, together with mechanisms skewing positive energy balance, contribute to why obese individuals struggle to maintain weight loss [43].

3.1 Brown Adipose Tissue

An evolutionary shift roughly 100 million years ago allowed placental mammals to thrive in cold regions of the Earth [44]. This development led to the emergence of BAT, a specialized organ that generates heat through non-shivering thermogenesis (NST) using energy from macronutrients. This is independent of shivering thermogenesis, where heat is produced by muscular contraction. The understanding of BAT as thermogenic tissue stemmed from morphological changes in BAT when animals were exposed to cold [45]. In the late 1970s, studies mapped tissue blood flow using radiolabeled microspheres to quantify heat output *in vivo*. Despite its small total mass at 1-2% of body weight, BAT accounted for 60% of heat output in cold-acclimated rats, while skeletal muscle was responsible for only 12% [46,47]. BAT became accepted as the primary anatomical site of NST in cold-adapted animals, hibernators and neonates when environmental temperatures fell below the thermoneutral range [48, 49]. Thermoneutrality (TN) is defined as the ambient temperature at which an organism does not generate or lose heat and metabolic rate is at a minimum.

Intriguingly, BAT forms during embryonic development and is highly abundant in human babies. Newborns possess large interscapular and perirenal BAT depots, constituting approximately 5% of their body weight [50]. Due to their large body surface area to weight ratio, their body heat is lost rapidly when exposed to cold. Moreover, they are unable to shiver and thus cannot perform shivering thermogenesis to regulate body temperature. These factors increase the importance of NST to provide heat under cold environments encountered at birth and explain BAT enrichment in newborns.

For decades BAT was thought to be housed primarily in infants and young children. It was widely accepted that BAT was essentially nonexistent and without physiologic relevance in adult humans. Conventional views changed in 2009 when multiple studies unequivocally demonstrated the high incidence of metabolically active BAT in adult humans analyzing 18F-fluorodeoxyglucose (18F-FDG) positron-emission tomographic and computed tomographic (PET–CT) scans [51, 52, 53]. In adults, substantial active BAT depots were typically found in the cervical–supraclavicular region. However, there was great variation with respect to abundance and metabolic activity. Smaller BAT depots were also present in axillary, peri-aortic, paraspinal, and suprarenal regions. In another 2009 study, cold exposure showed significant 18F-FDG uptake into adipose tissue of the

supraclavicular and paraspinal regions, suggesting NST in adult humans [53]. Interestingly, the amount of BAT was inversely correlated with BMI, especially in older individuals, suggesting a potential role of BAT in adult human EE and adiposity.

The role of BAT in regulating body temperature during cold exposure has been extensively studied in small rodents. BAT is present in rodents from birth and continues to play a significant role in NST throughout their lives. However, the involvement of BAT in EE and adiposity was contested until a seminal study conducted by Rothwell and Stock in 1979 [54]. To begin, they observed rats fed a high-calorie diet ('cafeteria diet' composed of junk foods high in fats and sugars) gained less weight than expected from calorie intake. BAT thermogenesis was induced, and EE increased relative to control-fed rats. Additionally, this level of BAT activation in 'cafeteria' fed rats was comparable to BAT activation during cold exposure. As a result, they proposed that the excess unaccounted calories that did not contribute to weight gain were burned off by the induction of BAT thermogenesis. The increase in EE due to the generation of heat following a high-calorie diet was referred to as "diet-induced thermogenesis" (DIT). Altogether, DIT increased EE, which resulted in lowered metabolic efficiency, thus supporting a protective role of BAT thermogenesis towards resisting excessive weight gain. This study absolved controversy regarding the role of BAT in DIT and laid the groundwork for further research into this energetically wasteful tissue and its potential applications in combating obesity.

Therefore, the unequivocal demonstration of human adult brown fat in the late 2000s provided the missing link and ignited an explosion in the literature investigating BAT as an anti-obesity target. These data dovetailed with studies in animal and human models that demonstrated defective BAT thermogenesis caused increased susceptibility to diet-induced obesity [55]. As a proof of concept, human BAT was also activated following carbohydrate-rich meals [56]. In addition, BAT mass was inversely correlated with BMI, while BAT activation was associated with a healthier metabolic phenotype, such as insulin sensitivity [2]. Altogether, these findings strongly support the potential of BAT to equilibrate the energy imbalance observed in millions of obese individuals and have reinvigorated interest in understanding the pathways that promote and inhibit brown fat thermogenesis.

3.2 Brown Adipocyte Development

Brown adipocytes are the functional thermogenic unit and most abundant cell type of BAT. It was previously believed that brown and white adipocytes shared a common progenitor. However, in the late 2000s, Seale *et al.* showed that the transcriptional regulator PRDM16 (PRD1-BF1-RIZ1 homologous domain containing 16) controls the bidirectional cell fate between skeletal myoblasts and brown adipocytes [58]. This discovery indicated that brown fat and skeletal muscle share a common Pax7+Myf5+ progenitor from the embryonic mesoderm. As a result, brown fat precursor cells express genes similar to those found in muscle cells and have related mitochondrial proteomes [57, 58]. Notably, PRDM16 knockdown in primary brown adipocytes triggered a phenotypic switch to skeletal muscle, while overexpression of PRDM16 in myoblasts switched them to brown adipocytes. It was later found that EBF2 (Early B Cell Factor 2) cooperates with PPARγ (Peroxisome proliferator-activated receptor gamma) in Pax7+Myf5+ progenitors to promote the expression of PRDM16 and facilitate differentiation of brown preadipocytes to mature brown adipocytes [59]. In parallel, there is increased expression of genes related to lipid metabolism and mitochondrial function [60]. Mature brown adipocytes are morphologically distinct from white adipocytes, as they are densely packed with mitochondria and contain small multilocular LDs. It remains unknown whether Myf5+ stem cells are multipotent or whether distinct pools of Myf5-expressing precursors contribute to muscle and brown fat. The thermogenic capacity of BAT depends on the total number of brown adipocytes, the degree of differentiation of the tissue, and mitochondrial density. Importantly, the respiratory activity of brown adipocytes does not increase under basal conditions (i.e. TN) and requires activation to achieve maximal thermogenic capacity.

3.3 Sympathetic Activation of Brown Adipose Tissue

BAT is densely innervated with postganglionic neurons of the sympathetic nervous system (SNS) [61, 62]. During cold exposure or following a high-calorie meal, sympathetic nerve fibres release the catecholamine noradrenaline (NA). NA is the most physiologically

relevant activator of ligand-mediated facultative and adaptive adipocyte thermogenesis [63, 64]. Facultative or acute thermogenesis occurs by uncoupling oxidative phosphorylation. In contrast, adaptive or long-term thermogenesis relies on transcriptional changes that increase thermogenic capacity (i.e. expression of thermogenic proteins, differentiation and proliferation of brown preadipocytes). Released NA agonizes adrenergic receptors (ARs) on BAT and initiates a downstream signaling cascade to stimulate thermogenesis. Thus, intact innervation is essential for NST and DIT. An interesting proof of concept is observed in rare catecholamine-secreting tumours, such as paragangliomas and pheochromocytomas that form in adrenal glands [65]. In healthy individuals, the adrenal medulla produces catecholamines such as NA upon SNS activation. However, in cases of paragangliomas, NA can be chronically produced under basal conditions. As a result, patients presenting with pheochromocytoma often experience significant weight loss due to resultant BAT activation.

ARs are G-protein-coupled receptors (GPCRs) and can be further classified as α -ARs linked to Gq proteins and β-ARs linked to Gs proteins [66]. Of the two pathways, β-AR signalling has dominated the literature regarding the sympathetic activation of adipocytes. G proteins have seven transmembrane α-helices and three intracellular subunits (α, β, and γ). When NA binds β-AR, primarily β3-adrenergic receptors (β3-AR) on brown adipocytes, a conformational change allows the α-subunit to dissociate from the βγ-complex tethered to the cell membrane [67]. The activated GPCR exchanges guanosine diphosphate (GDP) bound to the α-subunit with guanosine triphosphate (GTP). The active α-subunit then interacts with its effector protein, adenylyl cyclase (AC). Next, AC converts adenosine triphosphate (ATP) to secondary messenger, cAMP. One of the primary targets of cAMP is Protein Kinase A (PKA). In brown adipocytes, PKA activates HSL, a key lipolytic enzyme, via phosphorylation at three serine residues [68]. Facultative activation of lipolysis liberates FFAs from multilocular LDs to serve as substrates for β-oxidation. Each round of β-oxidation produces equivalents of NADH and $FADH_2$ for the electron transport chain (ETC) to increase respiratory capacity for thermogenesis [69]. In addition, activated PKA also drives transcriptional responses of a thermogenic gene program in brown adipocytes through the activity of phosphorylated cAMP-response element binding protein (CREB) [70, 71]. One of the targets of CREB is

peroxisome proliferator-activated receptor gamma (PPARγ) coactivator-1α (PGC-1α) [72]. Pgc-1α is regarded as the master regulator of mitochondrial biogenesis and oxidative metabolism. Pgc-1α binds DNA to control the activation of brown adipocytes through interactions with PPARγ and PPARα [73]. While PPARγ and PPARα can compensate for one another, Pgc-1α is essential for sympathetic activation [73, 74, 75]. Moreover, Pgc-1α activates estrogen-related receptors (ERRα and ERRγ) downstream, which further regulates the transcription of genes essential for oxidative and thermogenic capacity [76].

It is well-established that NA has an affinity for various GPCRs in addition to β3-AR [77]. On brown adipocytes, NA can bind three central receptors: α1, α-2, and β-AR [77]. However, the understanding of the Gq pathway linked to α-ARs and how it contributes to adipocyte thermogenesis remains incomplete. When NA binds α-AR, specifically α1-adrenergic receptors (α1-AR) on brown adipocytes, a similar conformation change occurs where the α-subunit dissociates from the βγ-complex and the swaps GDP for GTP. Next, the α-subunit activates Phospholipase C (PLC) instead of AC. PLC then hydrolyzes phosphatidylinositol 4,5-bisphosphate (PIP_2), an essential lipid in metabolic processes [78]. This reaction yields secondary messengers: inositolphospholipase (IP_3) and diacylglycerol (DAG). IP_3 stimulates the calcium release from the endoplasmic reticulum and activates adipogenesis through calmodulin [79]. Meanwhile, DAG remains anchored to the cell membrane and activates Protein Kinase C (PKC), which phosphorylates transcription factors and histone modifiers [80]. A 2016 study by Klepac *et al.* showed that the Gq signalling pathway inhibits brown and beige (white adipocytes with brown adipocyte characteristics) adipose tissue [78]. However, with this logic, selective activation of the Gs pathway (i.e. via CL 316,243, a selective β3-AR agonist) should increase thermogenic capacity compared to NA alone, which activates both Gs and Gq pathways. However, this is not the case. Although studies with obese mice showed robust reductions in adiposity when treated with a CL 316,243 [81], the effects were lower relative to NA-stimulated thermogenesis. Another recent study elegantly demonstrated that the integration of Gq and Gs pathways results in a synergistic effect that maximizes adipocyte thermogenesis through a mechanism dependent on increased transcription of thermogenic effector proteins [82]. Subsequent studies are investigating the cooperative effect of Gs and Gq activation on ameliorating diet-induced obesity.

Overall, sympathetic activation of BAT allows brown adipocytes to circumvent the usual limitations of mitochondrial respiratory control, which typically dictate substrate-level phosphorylation and thereby achieve maximal thermogenic capacity.

3.3 Mitochondrial Respiratory Control

BAT is highly vascularized to ensure the extraordinary levels of metabolites that undergo cellular respiration receive an optimal supply of oxygen [61, 62]. BAT depots are a catabolic sink for glucose, fatty acids, and branched-chain amino acids (BCAAs) to the point where BAT activation leads to improvements in glucose homeostasis, lipid homeostasis, and BCAA clearance in rodents and humans [83]. In order to meet such high metabolic requirements, brown adipocytes are densely packed with mitochondria. Interestingly, 'brown' fat is a result of this high mitochondrial content, which contains significant amounts of iron, giving the fat its distinctive colour. In eukaryotes, oxidative phosphorylation is executed by mitochondria and provides the most efficient way to generate ATP.

The mitochondrial chemiosmotic theory provides the principles for understanding the electron transport chain (ETC) and respiratory control. Free energy released from the oxidation of metabolites is coupled with the reduction of high-energy electron carriers (NADH and $FADH_2$). These electron-rich byproducts then undergo oxidation themselves in a series of oxidation-reduction reactions connected to the ETC. The ETC is found in the inner mitochondrial membrane in eukaryotes and consists of a series of protein complexes (I, II, III, IV, V) along with other mobile conjugated proteins (Coenzyme Q & Cytochrome C). In the mitochondrial matrix, NADH is oxidized to NAD^+ at Complex I (NADH-CoQ oxidoreductase), and lost electrons are transferred along the ETC. Electrons lost from $FADH_2$ are similarly transferred along the ETC, however, oxidation of $FADH_2$ to FAD occurs at Complex II (Succinate-CoQ oxidoreductase). In the final oxidation-reduction reaction, electrons are given to diatomic oxygen (O_2) in the form of hydride ions and water is formed. As electron pairs are transferred to increasing reduction potentials along the ETC, each subsequent oxidation-reduction reaction releases free energy that is coupled to the movement of protons out of the mitochondrial matrix into the

intermembrane space via protein complexes (I, III, IV) that are also proton pumps. Altogether mitochondrial respiration results in the establishment of an electrochemical gradient known as the protonmotive force along the inner mitochondrial membrane. As more NADH and $FADH_2$ are oxidized, the voltage difference between the intermembrane space and matrix increases. Complex V (ATP synthase) harnesses the potential energy stored in the electrochemical gradient for ATP synthesis while concomitantly releasing protons back into the mitochondrial matrix.

ATP synthase is composed of an F0 subunit embedded into the inner membrane and an F1 subunit that protrudes into the matrix. The F0 portion interacts with the protonmotive force and functions as an ion channel, allowing protons to travel down their gradient toward the matrix. This process is exergonic as protons experience a decrease in potential energy. The F1 portion utilizes the free energy released as a means of forming a high-energy phosphoanhydride bond between adenosine diphosphate (ADP) and inorganic phosphate (Pi) to produce ATP. This process is referred to as chemiosmotic coupling and describes a direct relationship between the electrochemical gradient and ATP synthesis. Another school of thought is called conformational coupling and suggests an indirect relationship between the electrochemical gradient and ATP synthesis. More specifically, the flow of protons through F0 drives the rotation of F1 within a stationary compartment and facilitates the harnessing of the gradient energy for ATP synthesis.

ATP synthesis is dependent on a stoichiometric relationship with regard to the number of electron carriers, protons pumped into the intermembrane space, and protons that return to the matrix via ATP synthase. With an understanding of respiratory control, EE can be manipulated by increasing ATP turnover to increase ADP availability or by uncoupling the ETC from ATP synthesis. Uncouplers are compounds that prevent ATP synthesis without affecting the ETC. For example, chemical uncoupler 2,4-dinitrophenol (DNP) allows protons to leak from the intermembrane space into the matrix rather than through ATP synthase [84]. The energy produced from the loss of electric potential energy is released as heat. This significantly decreases the efficiency of the ETC. ATP synthesis decreases and ADP accumulates, the body responds to this perceived lack of energy by increasing O_2 consumption, NADH oxidation, and thus EE. In the 1930s, mitochondrial uncoupling had been tried as a weight-loss therapy. DNP was used widely as a diet pill

to treat obesity, providing proof-of-concept support for mitochondrial uncoupling as an approach to weight loss. However, dosages vary widely amongst people and at high doses, unregulated systemic respiratory uncoupling caused hyperthermia and even death [84]. Although pharmaceutically increasing BAT activity holds promise to one day combat obesity, treatments should be selective to brown fat cells.

3.4 UCP1-Dependent Thermogenesis

The most well-studied thermogenic system in BAT relies on uncoupling substrate oxidation from ATP synthesis through uncoupling protein 1 (UCP1) mediated proton leak [3]. UCP1 was first discovered by Nicholls and colleagues in 1976 [85]. UCP1 is a long-chain fatty acid (LCFA) anion/H+ symporter localized in the inner mitochondrial membrane that is selectively expressed in brown adipocytes. UCP1 antagonizes the proton motive force established by the ETC [86, 87, 88]. This allows protons to travel down their concentration gradient back into the mitochondrial matrix and circumvent ATP synthase. The free energy that is normally coupled to the phosphorylation of ADP is now dissipated as heat in activated brown adipocytes.

It is important to note that UCP1 proton conductance is inactive under basal (i.e. unstimulated) conditions. More specifically, physiological concentrations of purine nucleotides (i.e. GDP, GTP, ADP, ATP) bind and competitively inhibit UCP1 [89]. Cryo-electron microscopy (EM) has recently revealed that purine inhibitors directly bind and prevent conformational changes in UCP1 essential to facilitate proton leak [90]. SNS activation (i.e. by cold, diet, or pharmacologically), specifically through the β3-AR Gs pathway is multifaceted. First, it results in acute activation of UCP1 where inhibition is lifted. Second, it increases Ucp1 transcription and subsequent protein synthesis for adaptive thermogenesis [91]. As previously mentioned, Gs signalling in brown adipocytes leads to lipolysis and the liberation of FFAs. Of the FFAs, the LCFAs specifically are direct allosteric activators of UCP1. Furthermore, LCFAs bind UCP1 with greater affinity than competitive purine inhibitors and can overcome inhibition [89]. Once bound, mitochondrial respiration becomes uncoupled, leading to increased respiration and thermogenesis *in vivo* [3].

3.5 UCP1-Independent Thermogenesis

It was long thought that UCP1 was the only thermogenic mechanism in brown adipocytes. This understanding stemmed from a study in which UCP1-knockout (KO) mice of a pure genetic background succumbed to hypothermia upon acute cold exposure – suggesting that NST was defective without UCP1 [92]. However, if UCP1-KO were gradually acclimated to the cold, they survived [93]. In addition, UCP1-KO mice on a mixed genetic background can also maintain body temperature like WT mice regardless of acute or gradual cold exposure [94]. The ability of some UCP1-KO mice to regulate body temperature suggests alternative thermogenic pathways are active in these mice.

Nevertheless, the argument from proponents of UCP1-dependent thermogenesis was that these mice were able to compensate for the lack of NST by relying on shivering thermogenesis for thermal homeostasis and not alternative thermogenic pathway(s). This argument makes some key assumptions that have since been disproven. First and foremost, the degree of shivering between wild-type (WT) and UCP1-KO mice on a congenic background was quantitatively identical. Secondly, there was no difference in levels of shivering in UCP1-KO mice when exposed to cold acutely or gradually [92]. Therefore, it is unlikely that shivering thermogenesis contributes to explaining the difference in survival.

The UCP1-KO murine models employed in these studies were constitutive KOs developed by Enerback, Kozak, and colleagues. Further investigation of this KO model in recent years using Cryo-EM has revealed that constitutive UCP1-KOs experience mitochondrial disruptions that extend beyond UCP1 deletion [95]. More specifically, most components of the ETC and maximal respiratory capacity in BAT are significantly reduced compared to WT BAT. As a result, impaired BAT mitochondrial biology in this model may have contributed to underestimating the dispensability of UCP1. To account for this limitation moving forward, Rahbani *et al.* developed an inducible adipocyte-specific UCP1-KO model that evades secondary changes beyond UCP1 [96].

Recently, there has been more resounding evidence in favour of UCP1-independent thermogenesis. For example, mice with nearly complete ablation for BAT

developed obesity on a chow diet, whereas UCP1-KO mice were protected from diet-induced obesity even on a high-fat diet [97]. This was highly unexpected, given the involvement of BAT in DIT and the preconceived notion that UCP1 was the sole thermogenic effector. This suggested thermogenic pathway(s) were lost in brown-fat ablated mice that were still present in UCP1-KO mice. Another study indicated that UCP1-KO BAT experiences a significant increase in temperature following NA treatment – corroborating studies of cold-tolerant UCP1-KO mice [98]. Altogether, these data demonstrated that UCP1 is expendable for NST and hinted towards alternative and independent thermogenic pathway(s) in BAT.

The last decade has seen the identification of UCP1-independent thermogenic pathways: creatine-dependent substrate cycling, lipolysis/re-esterification cycling, and sarcoplasmic/endoplasmic reticulum-based calcium cycling [4, 5, 6, 99, 100, 101]. A common theme is the futile nature of these cycles. how they function as ATP sinks without performing mechanical or chemical work. Futile ATP consumption is thermogenic and drives mitochondrial respiration to establish the ATP pool and increase EE. Futile cycle activity is challenging to examine *in vivo*, but the field is developing elegant methods to identify underlying molecular and regulatory mechanisms along with physiological relevance. The present review will focus on the futile creatine cycle (FCC).

3.6 Thermogenic futile creatine cycling

Creatine (Cr) canonically serves as a rapid energy source for muscle fibres during short-duration, high-intensity activities. ATP is quickly formed from the direct phosphorylation of ADP using phosphocreatine (PCr). The PCr and ADP pool is regenerated using a tissue-specific creatine kinase (CK) and exists in equilibrium with Cr and ATP. More specifically, the metabolic usage of Cr exists in a 1:1 stoichiometric relationship with ATP. For example, the addition of one mole of Cr to coupled mitochondria will result in one mole of ADP and PCr production via CK activity [102]. Interestingly, a 1976 study performed by Berlet *et al.* highlighted a potential non-canonical role of Cr in BAT [103]. They found that the import rate of Cr into BAT was comparable to skeletal muscle. Furthermore, brown adipocytes exhibited CK activity; however, the BAT CK isoenzyme(s)

remained elusive. Nearly 20 years later, a reduction in Cr levels was linked to dysfunctional thermal homeostasis *in vivo* via an unknown mechanism [104, 105]. Albeit a Cr-dependent thermogenic pathway was not insinuated until much later.

In 2015 Kazak *et al.* uncovered the first signs of a futile creatine cycle (FCC) in BAT linked to EE and thermogenesis [4]. As mentioned in most cell types, the phosphorylation/dephosphorylation reaction of Cr/PCr coupled to ATP/ADP exhibits a strict 1:1 stoichiometric relationship. Surprisingly, this was not the case in thermogenic adipocytes; rather, Cr-stimulated mitochondrial respiration released a molar excess of ADP relative to Cr [4, 106]. More specifically, CK phosphorylates Cr into PCr and liberates ADP. The resultant PCr was hypothesized to be immediately hydrolyzed by a phosphatase, leading to the regeneration of Cr. Therefore, the same molecule of Cr can serve as a substrate for CK again to generate PCr and liberate ADP. Here the futile nature of the cycle becomes evident. Phosphorylation of Cr depletes the ATP pool and shifts the equilibrium towards ADP. As ADP accumulates, mitochondria respond to this perceived lack of energy by driving respiration and releasing heat as a byproduct. Each molecule of Cr liberates more than one molecule of ADP, hence the super-stoichiometric molar excess of ADP liberation. Importantly, creatine-dependent respiratory response occurred in adipocyte mitochondria only when ADP was limiting – which is expected under physiological conditions [4]. Overall, these findings postulated the presence of a mitochondrial Cr cycle to drive respiration and thermogenesis. The key CK isoenzyme(s) and proposed PCr phosphatase controlling FCC-mediated ATP turnover would not be identified for a few more years.

In subsequent studies, Kazak *et al.* aimed to investigate the physiological relevance of thermogenic creatine cycling. The Cr pool in adipocytes is controlled by intracellular synthesis and absorption from circulation [107, 108]. Selective inactivation of glycine amidinotransferase (GATM), the rate-limiting enzyme of creatine biosynthesis, depleted Cr in thermogenic adipocytes and increased susceptibility to diet-induced obesity [107]. Moreover, fat-specific genetic and pharmacological inhibition of Cr transporter SLC6A8 also increased susceptibility to diet-induced obesity [108]. Importantly, these phenotypes were observed in the presence of functional UCP1. If creatine-dependent thermogenesis was only initiated in the absence of UCP1, it would

not be a true UCP1-independent thermogenic pathway. Together, these studies provided substantial support for the *in vivo* relevance of creatine metabolism in adaptive thermogenesis.

Finally, in 2021 the two key effectors of the FCC were respectively characterized in two independent studies performed by Rahbani *et al.* and Sun *et al.* [8, 9]. Creatine kinase B (CKB; encoded by Ckb) was identified as the key CK isozyme, and tissue non-specific alkaline phosphatase (TNAP; encoded by Alpl) was identified as the phosphocreatine phosphatase [8, 9]. The coordinated activities of these enzymes establish the FCC and contribute to adipocyte thermogenesis by triggering ATP turnover in both mice and humans. CKB and TNAP respectively catalyze the phosphorylation/dephosphorylation cycle of creatine/phosphocreatine, which releases a super-stoichiometric quantity of ADP. CKB was imperative for FCC-mediated thermogenesis and trafficked to mitochondria using an internal mitochondrial targeting sequence [8]. TNAP was also localized to the mitochondria in thermogenic adipocytes, unlike other cells where it is found in the cytosol [9]. These data further confirmed that FCC indeed occurs in mitochondria. Independent adipocyte selective genetic ablation of CKB and TNAP also decreased whole-body EE and increased susceptibility to diet-induced obesity [8, 9].

Once CKB and TNAP were identified, the next research question that stood out concerned the enzymatic regulation of the FCC effectors under facultative (acute) and adaptive (chronic) conditions. In 2022, Rahbani *et al.* showed that Ckb and Alpl expression was dependent on coordinated α1-AR and β3-AR signalling – linking the Gq pathway to the FCC [82]. This was in contract with Ucp1 expression, which is downstream of β3-AR signalling linked to the Gs pathway [82]. Furthermore, transcriptional regulation of FCC effectors *in vivo* was dependent on transcription factors: early B cell factors (EBFs), estrogen-related receptors (ERRs), and PGC1α [82].

The current state of the field aims to elucidate how CKB and TNAP activity are regulated on an enzymatic level to rapidly control facultative thermogenic demands. Are there any allosteric or post-translational modifications (PTMs) that occur to CKB, TNAP, or another unknown protein in the pathway? For instance, PTMs have been shown to regulate CK activity in some cell types but have not been identified in any physiological

setting related to CKB [109]. Alternatively, some alcohol acceptors have been shown to increase the reaction kinetics of TNAP-mediated phosphate hydrolysis [110]. The potential endogenous phosphate acceptor substrate of TNAP in brown fat is unknown. Moreover, do these enzymes undergo any fat-specific modifications that render them more susceptible to chemical or genetic activation? These underlying processes that regulate facultative (rapid) activation of FCC-mediated thermogenesis remain unknown and are the next step to one day harness the FCC to combat obesity.

Chapter 4: Aquaporins

Aquaporins are a family of transmembrane proteins that bidirectionally transport water across cell membranes via facilitated diffusion. The flow of water is dependent on the osmotic gradient and thus flows from areas of low to high concentration gradients to achieve homeostasis. The first aquaporin, initially named CHIP 28, was discovered by Peter Agre and colleagues in 1992 by serendipity [111]. Agre came across CHIP 28, later renamed aquaporin 1 (AQP1) while investigating red blood cell (RBC) membrane proteins. Aquaporins were found to be ubiquitously expressed and identified in bacteria, fungi, plants, and animals. In 1998, AQP3 was identified as another aquaporin isoform in RBCs, but instead of water, it transported glycerol via facilitated diffusion [112]. This created a new subset within the AQP family known as aquaglyceroporins. Thus far, 13 mammalian aquaporins have been discovered, 11 of which are expressed in mice and all 13 in humans [113]. AQP 0, 1, 2, 4, 5, 6, & 8 are categorized as classical aquaporins as they only transport water. Current members of the aquaglyceroporin family include AQP 3, 7, 9, & 10, and they transport water and glycerol with variable kinetics. AQP 11 and 12 are classified as unorthodox aquaporins because their permeability to water and glycerol varies and has not been extensively studied [114].

The crystal structures of six of the 13 mammalian aquaporins have been established and are relatively well-conserved between isoforms. Aquaporins are comprised of six membrane-spanning helices and the quaternary structure exists as homotetramers within the cell membrane. Each monomer creates one pore, and when all four monomers are arranged as a tetramer, a fifth central pore is formed [115]. High-

resolution X-ray crystallography has revealed that channel pore size can vary between isoforms, but all are tightly regulated to ensure only water and/or glycerol is transported [116].

Aquaporins are variably expressed throughout different tissues, but at least one isoform is predominant in each organ system [114]. Furthermore, their dysfunction is associated with a myriad of diseases. For example, AQP1 is highly abundant in kidneys, and tumours with AQP1 deficiency have increased angiogenesis, invasion, metastasis, and growth [117]. AQP1 silencing using RNA interference has been shown to reduce angiogenesis-dependent tumour growth in an *in vivo* melanoma model [118]. Therefore, manipulating AQP expression through genetic, pharmacological, transcriptional, or translational means can potentially be utilized as treatments – as indicated by recent research [113].

Interestingly, aquaporins have also been linked to obesity and are hypothesized to have a role in TAG hydrolysis. As mentioned in Chapter 2, the primary source of glycerol within adipocytes arises from the hydrolysis of triglyceride stores following lipolysis under fasted conditions. FFAs are also released and undergo β-oxidation, but when glycerol accumulates, it is exported out of adipocytes by aquaglyceroporins [11]. The bulk of glycerol travels through the bloodstream to the liver before it is taken up into the liver via hepatocyte-specific aquaglyceroporin, AQP9 [120]. Next, glycerol is converted to glycerol-3-phosphate (G3P) by glycerol kinase (GK). G3P is then converted to dihydroxyacetone phosphate (DHAP) by triose phosphate isomerase (TPI) and serves as an intermediate for gluconeogenesis [121]. In the fed state, glycerol is imported into adipocytes via aquaglyceroporins and serves as an intermediate for TAG synthesis to replenish lipid stores. The aquaglyceroporin found in adipocytes is thought to be AQP7 [119, 121, 122].

To investigate the effects of AQP7 depletion on adipocytes, previous studies have used global AQP7-KO mouse models [119, 121, 122]. In 2004 Maeda *et al.* found that AQP7 deletion resulted in a decrease in glycerol concentrations in plasma under fasted conditions [122]. However, because a global KO was used, it is unclear if this was due to a phenotype observed in adipocytes and not another tissue that unknowingly expressed AQP7. Another study in 2005 by Hara-Chikuma *et al.* found that AQP7-KO mice

developed diet-induced obesity and insulin resistance compared to WT mice on the same diet [119]. Their rationale was that AQP7 deletion resulted in glycerol accumulation and caused increased TAG synthesis. Another 2005 study performed by Hibuse *et al.* independently confirmed these findings [121]. More specifically, they found that GK activity was increased in AQP7-KO mice, which accelerated TAG synthesis and eventually led to obesity. These studies were the first to highlight AQP7 as a potential therapeutic target for obesity. Selective overexpression of AQP7 in adipocytes may reduce adipocyte hypertrophy and potentially reduce fat mass in obese individuals.

Despite these studies linking AQP7 and glycerol to obesity, a complete understanding of AQP7 in glycerol transport in adipocytes remains unclear. Given the widespread expression of aquaporins in various tissues, it is uncertain whether AQP7 is the only isoform involved in this process. Additionally, it is unknown if the expression pattern of AQP7 varies between brown and white adipocytes, as previous studies did not differentiate between these two highly distinct adipose tissue depots. Furthermore, the use of global knockout models in these studies prevented the pinpointing of AQP7's specific effects on brown adipocytes. Altogether, the role of aquaporins in brown adipocytes currently remains an avenue for discovery.

MATERIALS & METHODS

Cell culture

HEK293A and HEK293T (Human embryonic kidney 293) cells were cultured in Dulbecco's Modified Eagle's Medium (DMEM; Wisent), supplemented with 10% fetal bovine serum (FBS; Wisent) and 1% penicillin-streptomycin (P/S; Wisent) at 5% CO_2. Immortalized $Ckb^{fl/fl}$ preadipocytes were immortalized in-house as previously described [8]. Immortalized $Ckb^{fl/fl}$ preadipocytes were cultured in DMEM/F-12 GlutaMax (ThermoFisher), supplemented with 10% FBS (Millipore Sigma) and 1% P/S at 10% CO_2. Cell lines were tested for mycoplasma contamination.

Brown adipocyte differentiation

Brown preadipocytes were grown to post-confluency and induced to differentiate with an adipogenic cocktail (1 µM rosiglitazone, 1 nM T_3, 0.114 µg/ml insulin, 0.5 mM 3-isobutyl-1-methylxanthine (IBMX), 5 µM dexamethasone, 125 µM indomethacin). After 48 h media was changed to a maintenance cocktail (1 µM rosiglitazone, 1 nM T_3, 0.5 µg/mL insulin) and re-supplemented every 48 h. Adipocytes were fully differentiated six days after initial induction (seven days if cells underwent reverse transfection).

RNA extraction and quantitative RT-PCR

Total RNA extraction from cell and flash-frozen tissue (homogenized using TissueLyser II (Qiagen)) samples was performed using TRIzol reagent (Invitrogen) followed by RNeasy Mini Kit (Qiagen) as per the manufacturer's instructions. RNA concentrations were determined using a NanoDrop 2000 Spectrophotometer (ThermoFischer). 1 µg of purified RNA was reverse transcribed into cDNA using a High-Capacity cDNA Reverse Transcription kit (Applied Biosystems). 20 ng of obtained cDNA was mixed with 150 nmol of forward/reverse primer pairs and GoTaq qPCR Master Mix (Promega). qPCR reactions were performed in a 384-well plate using a CFX384 Real-time PCR system (Bio-Rad).

Raw Ct values were collected using CFX Maestro software and analyzed using the ΔΔCt method. *Ppib* or *Rps18* mRNA served as the reference gene. Primer sequences can be found in Table 2.0.

Western blotting and densitometry

Cell and flash-frozen tissue (homogenized using TissueLyser II (Qiagen)) samples were collected in adipocyte lysis buffer (50 mM Tris pH 7.4, 500 mM NaCl, 1% IGEPAL, 20% glycerol, 2 mM EDTA) supplemented with a cocktail of protease inhibitors (Roche). Homogenates were centrifuged (16000 g for 10 min at 4°C) and the protein content of the supernatant was determined using bicinchoninic acid assay (BCA; Pierce). 10 µg of protein lysate was denatured for 10 min at 95°C (or 20 min at 37°C for membrane proteins of interest) in Laemmli buffer (60 mM Tris, pH 6.8, 2% SDS, 10% glycerol, 0.05% bromophenol blue, 0.7 M β-mercaptoethanol). Samples were subjected to electrophoresis on 10% Tris/Glycine SDS-PAGE gels and transferred onto polyvinylidene difluoride (PVDF) membranes. Membranes were blocked using tris-buffered saline (TBS) with 0.005% Tween-20 (TBS-T) containing 5% milk for 45 min; then incubated with primary antibodies overnight at 4°C and probed with secondary antibodies for 45 min at room temperature. Membranes underwent three-10 min TBS-T washes following primary and secondary antibody incubations. Signals were detected using Clarity Western ECL Substrates (Bio-Rad) and ChemiDoc Imaging System (Bio-Rad). Primary antibodies were diluted in TBS-T containing 5% BSA and 0.02% NaN_3; secondary antibodies were freshly diluted in TBS-T containing 5% milk. Antibodies and corresponding dilutions were as follows: VCL (Cell Signaling; cat. no. 13901; dilution: 1:5000), AQP7 (ThermoFischer; cat. no. PA1-28171; dilution: 1:1000), anti-rabbit (Promega; cat. no. W4011; dilution: 1:10000), anti-mouse (Promega; cat. no. W4021; dilution: 1:10000). Densitometry analyses were performed on ImageJ.

siRNA-mediated gene silencing

RNAi transfections were performed in a reverse transfection mode on day 3 of the brown adipocyte differentiation as previously described [123, 124]. First, a transfection mix containing OptiMEM I Reduced Serum Medium (Life Technologies) supplemented Lipofectamine RNAiMAX (Life Technologies) and siRNA (10 μM stock), was incubated for 20 min at room temperature. 6-well culture plates received 200 μL of transfection mix per well (188 μL OptiMEM, 6 μL Lipofectamine RNAiMAX, 6 μL siRNA). Seahorse XF96 culture plates received 15 μL of transfection mix per well (14 μL OptiMEM, 0.5 μL Lipofectamine RNAiMAX, 0.5 μL siRNA). In parallel, adipocytes differentiating in 10 cm plates were trypsinized, centrifuged (300 g for 5 min at room temperature), and resuspended in maintenance cocktail media (0.5 μg/mL insulin, 1 nM T_3). Cells were replated into corresponding formats already containing transfection mix. 6-well culture plates received a 2 mL suspension of 1.5 million cells per well, while Seahorse XF96 culture plates received a 90 μL cell suspension of 20000 cells per well. After 48 h, cells were re-fed with fresh maintenance cocktail media (day 5). After another 48 h adipocytes were fully differentiated and subjected to downstream assays (day 7). All siRNAs employed in this study were duplex siRNAs as follows: ON-TARGETplus Mouse Aqp7 (11832) SMARTPool siRNAs (Dharmacon; cat. no. 040993-01) or MISSION siRNA Universal Negative Control #1 (Sigma-Aldrich; cat. no. SIC001). Sequences for siRNA targeting can be found in Table 4.0.

Glycerol release assay

Adipocytes were cultured in 6-well plates and the release of glycerol into the medium was measured on day 6 (regular culture conditions) or 7 (siRNA-mediated knockdown) of differentiation. First, brown adipocytes were washed three times with DMEM/F-12 supplemented with 4% fatty-acid-free bovine serum albumin (BSA; Millipore Sigma) to remove trace amounts of glycerol in complete media. Cells were equilibrated in 4% BSA DMEM/F-12 for 90 min before incubation with 1 μM noradrenaline (NA; Sigma-Aldrich) for 2 hours at 37°C. Following incubation, conditioned media was collected to serve as the extracellular glycerol fraction, while adhered cells were resuspended in RIPA lysis buffer (50 mM Tris pH 8, 150 mM NaCl, 1% IGEPAL, 0.5% sodium deoxycholate, 0.1%

SDS, 2 mM EDTA) to serve as the intracellular glycerol fraction. Released glycerol was separated from adipocytes and cell debris by spinning (8000 g for 1 min at room temperature) through Ultrafree-MC Centrifugal Filter (Millipore Sigma, cat. no. UFC30LG25). Glycerol concentrations in the media and lysate were determined using a glycerol assay kit (Sigma-Aldrich, cat. no. MAK117) as per the manufacturer's instructions. All inhibitors were added 30 min before NA.

Seahorse XFe96 respirometry assay

Four days following reverse transfection, brown adipocyte oxygen consumption rate (OCR) was measured using XF96 Extracellular Flux Analyzer (Seahorse Bioscience) as previously described [125]. On experiment day, cells were washed with XF respiration base medium (Sigma-Aldrich, cat. no. D5030) supplemented with 2% BSA (Sigma-Aldrich, A9647), 25 mM glucose (Sigma-Aldrich, G7021), 31 mM NaCl (Sigma-Aldrich, S9888) (adjusted to pH 7.4) and equilibrated at 37°C in non-CO_2 incubator for 1 hour before first measurement. Seahorse cartridges were previously hydrated with XF calibrant solution overnight at 37°C in non-CO_2 incubator. One measurement cycle consisted of a 3 min "Mix", 0 min "Wait", and a 2 min "Measure" period. OCR was measured under basal conditions before drugs were injected in the following order: 1 μM norepinephrine (Sigma; A9512), 2.5 μM oligomycin (EMD Millipore; Cat# 495455), 0.5 mM 2,4-dinitrophenol (Sigma; D198501), and a mixture of 5 μM rotenone (Sigma; Cat#R8875) & 5 μM antimycin A (Sigma; A8674). All drugs were freshly prepared in supplemented XF respiration base medium and listed as final concentrations in wells. RNA was isolated from cells following the respiration assay and knockdown efficiency was determined by RT-qPCR. OCR analysis was performed on Agilent Seahorse XFe Analyzers and Wave 2.6 software.

Floated isolation of mature brown adipocytes

Mice were cervically dislocated and the interscapular fat depot was dissected. The two BAT depots were excised from the surrounding WAT and washed with PBS. This process was repeated for a total of 5 mice (same sex) for downstream respirometry assay. Next,

BAT depots were minced for 7 min, and the resulting homogenate was digested in in Krebs-Ringer Bicarbonate Modified Buffer (KRBMB; 135 mM NaCl, 5 mM KCl, 1 mM $CaCl_2$, 1 mM $MgCl_2$, 0.4 mM K_2HPO_4, 25 mM $NaHCO_3$, 20 mM HEPES) supplemented with freshly prepared isolation buffer (2 mg/mL Collagenase B (Roche 43779621), 1 mg/mL Soybean Trypsin Inhibitor (Worthington-Biochem LS003571), 10 mM Glucose (Sigma G7528), 4% fatty acid-free BSA). After 45 min at 37 °C with vortexing every 5 min while shaking at 150 cycles/min, the slurry was filtered through a 100 µm cell strainer. The filtrate was then washed with respiration buffer (DMEMF12 + 4% fatty acid-free BSA). Adipocytes were allowed to float for 20 min at room temperature and centrifuged (200 g for 5 min at room temperature); after another 5 min, pelleted smooth vascular fraction (SVF), cell debris, and infranatant were removed. After the third and final wash, mature adipocytes present under the fat layer were collected. Cell counts were determined using a Bright-Line Haemocytometer (Hausser Scientific).

Ex vivo respirometry of mature brown adipocytes using an oxygen electrode

Clark-type electrodes (Rank Bros) were used to determine oxygen consumption rates of freshly isolated mature brown adipocytes as previously described [82]. Following the initial setup and calibration of the apparatus as per the manufacturer's instructions, fresh respiration buffer (DMEMF12 + 4% fatty acid-free BSA) was loaded into each chamber and allowed to equilibrate to atmospheric oxygen levels. While continuously stirred, 10000 adipocytes were added to each chamber, before they were closed with a lid – totalling a volume of 700 µL. An initial basal respiration rate was recorded before subsequent metabolite-dependent and/or drug-dependent rates. Metabolites and drugs were added into continuously stirring chambers using Hamilton syringes: (1 mM/10 mM glycerol, 1 µM noradrenaline). Multiple electrodes were used in parallel to measure respiratory rates and all conditions were repeated on all electrodes in triplicates to account for electrode-specific bias. Rank Brothers Dual Digital model 20: Picolog 6 data logging software was used for data collection. Only the linear components of oxygen consumption rate traces were used for analysis using OriginLab software.

Plasmid DNA transformation and purification

10-50 ng plasmid DNA was transformed into homegrown DH5α or Stbl3 bacteria in LB culture via heat-shock at 42°C for 45 secs, added to 450 µL of SOC media (2% Tryptone, 0.5% Yeast Extract, 10 mM NaCl, 2.5 mM KCl, 10 mM $MgCl_2$, 10 mM $MgSO_4$, 20 mM Glucose) and incubated for 45 mins at 37°C on shaker. Bacteria were plated on Amp^+, $Puro^+$, or Kan^+ plates and grown overnight at 37°C. Plasmid DNA was purified from isolated colonies grown overnight in LB (100 µg/mL Amp/Puro/Kan) using Plasmid Mini, Midi, and Maxi kits as per the manufacturer's instructions (Qiagen). DNA concentration was determined using a NanoDrop 2000 spectrophotometer (ThermoFisher).

Lentiviral sgRNA cloning, production, and use

Single guide RNAs (sgRNA) were designed using top CRISPick (Genetic Perfusion Platform; GPP) candidate sequences and synthesized by Integrated DNA Technologies (IDT). Sequences for sgRNA targeting can be found in Table 3.0. Complementary DNA oligonucleotides were annealed to generate sgRNAs that were ligated into *BsmB*I digested lentiCRISPRv2 plasmid (Addgene: #52961) as previously described [126, 127]. Quick Ligase (NEB M2200S) reactions were validated via restriction digest (*BamH*I and *Pac*I), and products were subjected to electrophoresis on 1% agarose gels and imaged via ChemiDoc Imaging System (Bio-Rad). Integration of oligonucleotides into the backbone was confirmed using next-generation sequencing analysis and SnapGene software.

3 µg lentiCRISPRv2, 2.25 µg psPAX2 packaging vector (Addgene: #12260), and 0.1 µg pMD2.G envelope vector (Addgene: #12259) were co-transfected into each 10-cm plate of HEK293T cells at 70% confluency using Lipofectamine 2000 Transfection Reagent (Invitrogen) as per the manufacturer's protocol. Viral media was collected four times at 8 hr intervals 48 h post-transfection, centrifuged (300 g for 5 min at 4°C) to remove cell debris, and passed through a 0.45 µm filter. Viral supernatant was then concentrated via a polyethylene glycol (PEG)-based system as previously described [128, 129] before the viral pellet was resuspended in PBS and stored at -80°C.

Next, a viral titration was performed using a qPCR Lentivirus Titer Kit (abm LV900) as per the manufacturer's instructions. Lentiviral infections were done as previously described to establish CRISPR/Cas9 knockout lines in immortalized preadipocytes [128]. Briefly, preadipocytes were transduced with lentivirus at an MOI of ~30 with polybrene (8 µg/mL) or vehicle (negative selection control) and propagated for an additional 48 h. Cells were then treated with 3.5 mg/mL puromycin for 48 h to remove non-infected cells. Optimal puromycin concentration was determined via a titration curve for specific in-house strain of immortalized preadipocytes. After 48 h when non-infected control preadipocytes died, surviving cells were selected via limiting dilutions as previous described, grown to post-confluency and differentiated to day 6 [3]. Brown adipocytes were then collected with cold PBS without trypsinization and pelleted for validation via western blot.

Adeno-associated virus shRNA cloning and production

Short hairpin RNAs (shRNA) were designed using the Genetic Perfusion Platform (GPP) RNAi web tool and synthesized by Integrated DNA Technologies (IDT). Sequences for shRNA targeting can be found in Table 5.0. Complementary DNA oligonucleotides were annealed to generate shRNAs using NEBuffer r2.1 (New England Biolabs B6002) as per the manufacturer's instructions. pDIO-DSE-mCherry-PSE-MCS plasmid (Addgene: #129669) underwent restriction digest using *Avr*II and *EcoR*I-HF (New England Biolabs R0174, R3101) as per the manufacturer's instructions. 20-100 ng of digested plasmid backbone with a 3-fold molar excess of shRNA oligonucleotides were ligated using Instant Sticky-end Ligase master mix (NEB M0370L). Integration of oligonucleotides into the backbone was confirmed using next-generation sequencing analysis and SnapGene software.

HEK293A cells were grown to near confluency on 15-cm plates and co-transfected with: 2.5 mL OptiMEM I Reduced Serum Medium (Life Technologies), 10 µg pDIO-DSE-mCherry-PSE-MCS, 39.5 µg AAV- Cap8 vector pDP8 (PlasmidFactory GmbH, Germany, #pF478), 0.2 mg PEI (Polyscience 23966-1) as previously described [130]. 72 h post-transfection, viral media was harvested, centrifuged (3000 g for 15 min at 4°C) to remove

cell debris, and passed through a 0.22 µm filter. Viral supernatant was then concentrated using AAVanced Concentration Reagent (SBI cat # AAV110A-1) as per the manufacturer's instructions before the viral pellet was resuspended in PBS, flash frozen and stored at -80°C.

Next, viral stocks were tittered via qPCR as previously described [131]. Briefly, recombinant AAV (rAAV) samples underwent DNaseI (NEB M0303) treatment as per the manufacturer's instructions, to remove trace amounts of DNA coating the viral capsid. The viral rAAV genome was then extracted using RNA/DNA Extraction Reagent-ViralXpress kit (Millipore cat# 3095) as per the manufacturer's instructions. pDIO-DSE-mCherry-PSE-MCS backbone was digested using *Nhe*I-HF and serially diluted to establish a standard curve. Serial dilutions were also performed from rAAV samples. Sample or standard was mixed with GoTaq qPCR Master Mix (Promega) and 100 nm forward (GCTGGTCTCCAACTCCTAATC) & (AAATCAGAAGGACAGGGAAGG) reverse primer pairs. AAVs with a titer equal to or higher than 10^{11} genome copy/mL were used for *in vivo* injections – ensuring a maximal injection volume of 20 µL per brown adipose tissue depot.

rAAV gene delivery via surgical injection of interscapular BAT (iBAT)

Direct iBAT injections were performed as previously described [131]. Briefly, Adiponectin-Cre mice housed at room temperature were subcutaneously administered carprofen (20 mg/kg) 20 min before they were anesthetized via inhalation of isoflurane (3.5% at 0.5 L/min for induction, 2.5% at 0.5 L/min for maintenance) and placed in the prone position. The interscapular incision site was shaved and disinfected using Baxedin (2% chlorhexidine in 70% isopropanol). A 5 mm horizontal midline incision was made approximately 8 mm inferior to the skull base in the interscapular region through the skin and fascia. The fat pad covering the iBAT was visualized using blunt dissection and rAAV-pDIO-DSE-mCherry was injected into both iBAT depots via Hamilton syringe. A droplet of lidocaine was added to the surgical site before closing with surgical autoclips and glue. Mice were then injected with isotonic fluids (0.2 mL/10 g) subcutaneously and allowed to recover in clean cages at 22°C with access to a 37°C heating pad. For three days post-

operation, mice received carprofen (20 µg/g) and were monitored daily until autoclips were removed in 7-10 days. All experiments (indirect calorimetry) were performed at least 2 weeks after the surgery.

Indirect calorimetry in anesthetized mice post-operation

Indirect calorimetry for noradrenaline-stimulated thermogenesis in anesthetized mice was performed as previously described [96]. In brief, 2 weeks after iBAT injections mice were anesthetized by an intraperitoneal injection of Avertin (0.5 g/kg) and placed in the prone position into individual metabolic cages (Sable Systems International, Promethion high-definition behavioural phenotyping system) at 30°C. Data were collected from four mice in parallel. After 6 min of baseline energy expenditure measurements, cages were reopened and 20 µg (60 nmol) of noradrenaline (Sigma-Aldrich, A9512) was subcutaneously injected above the interscapular brown adipose tissue. NA-stimulated energy expenditure was allowed to reach its peak during the 30 min post-injection window of Avertin anesthesia. Avertin and noradrenaline stocks were prepared as previously described [10]. Data was processed with a 1 minute One-Click Macro (v2.51.0).

Animals

Mouse experiments were performed according to procedures approved by the Animal Resource Centre at McGill University and complied with guidelines set by the Canadian Council of Animal Care. Unless otherwise specified, mice were housed at 22 °C under a 12-h light/dark cycle and given free access to food and water. Litermate controls were used for all experiments unless otherwise indicated in figure legend. Mice were singly housed for cold exposure experiments and housing temperatures are indicated in figure legends. Wild-type C57BL/6N mice were purchased from Charles River (strain code: 027). AdipoqCre mice (B6;FVB-Tg(AdipoQ-Cre)1Evdr/J), stock 028020), maintained on a C57BL/6J background. Genotyping primer sequences for AdipoqCre: forward, 5′-ACG GAC AGA AGC ATT TTC CA-3′; AdipoqCre reverse, 5′-GGA TGT GCC ATG TGA GTC TG-3′.

Statistical analyses

All quantitative experiments are plotted as graphs with the mean ± standard error of the mean. Respective figure legends indicate number of independent experiments represented in data and statistic test used for significance. A p-value < 0.05 is flagged with one asterisk (*). A p-value < 0.01 is flagged with 2 asterisks (**). A p-value < 0.001 is flagged with three asterisks (***). A p-value < 0.0001 is flagged with 4 asterisks (****). A p-value > 0.05 is either unflagged or indicated with ns. (not significant). All statistical analyses were performed using Prism version 10 (Graphpad Software).

INTRODUCTION

Obesity rates are climbing globally, and if prevention and treatment are not improved, projections forecast more than half the world population will be overweight or obese by 2035 [1]. Not only does this epidemic create an economic burden, but obesity is also associated with various disorders ranging from cardiovascular diseases to certain cancers. In its simplest form, a chronic disparity between excess energy intake and minimal energy expenditure leads to the remodelling of the adipose tissue pool and, ultimately obesity. The adipose tissue pool is comprised of functionally distinct white adipose tissue (WAT) and brown adipose tissue (BAT). On the one hand, WAT is the primary site of energy storage and excessively accumulates in obesity. On the other hand, BAT maintains body temperature by generating heat from macronutrient-derived energy via non-shivering thermogenesis. Moreover, BAT abundance is associated with cardiometabolic health [2]. Thus, thermogenic BAT can be harnessed to stabilize the imbalance between energy intake and expenditure observed in obesity.

The most well-studied thermogenic system in BAT relies on proton leak mediated by uncoupling protein 1 (UCP1), which uncouples mitochondrial respiration for adenosine triphosphate (ATP) synthesis. Free fatty acids released from triglyceride stores physiologically activate UCP1 following noradrenaline-stimulated lipolysis [3]. Thermogenesis can also occur independently of UCP1 via futile substrate cycles that consume ATP without performing work. This includes creatine, lipid, and calcium cycling, which serve as metabolic sinks and contribute to increased energy expenditure in beige and brown adipocytes [4, 5, 6]. However, the activation mechanism(s) of UCP1-independent thermogenic pathways such as the futile creatine cycle (FCC) remain elusive.

The FCC contributes to adipocyte thermogenesis by triggering ATP turnover through the coordinated activities of creatine kinase B (CKB) and tissue non-specific alkaline phosphatase (TNAP) [7, 8, 9]. In the forward reaction, CKB hydrolyzes ATP to phosphorylate creatine, producing phosphocreatine and adenosine diphosphate (ADP). In the reverse reaction, TNAP hydrolyzes phosphocreatine to replenish the creatine pool for subsequent cycling. Importantly, this phosphorylation/dephosphorylation cycle of

creatine/phosphocreatine releases a super-stoichiometric quantity of ADP. This implies that each mole of creatine results in a molar excess of ADP liberation – further driving respiration and heat production. Employing biochemical and bioenergetic approaches, our laboratory recently identified glycerol, another lipolysis product, as an allosteric activator of TNAP. The presence of glycerol further amplified the super-stoichiometric quantity of ADP liberation and enhanced FCC activity.

A significant source of glycerol within brown adipocytes arises from the hydrolysis of triglyceride stores following noradrenaline-stimulated lipolysis [10]. When glycerol accumulates, it is exported out of adipocytes by a subset of aquaporins, called aquaglyceroporins. Aquaporins are a family of homologous intermembrane channels; aquaglyceroporins permeabilize water and glycerol via facilitated diffusion where permeability is dependent on glycerol concentration [11]. The objective of this project is to elucidate whether genetic manipulation of glycerol transport serves as a mode of rapid (facultative) FCC activation. Preventing glycerol efflux would trap glycerol intracellularly, thus presenting an opportunity to activate the FCC through enhanced TNAP catalytic activity rapidly. We hypothesize that the genetic trapping of glycerol in brown adipocytes will hyperactivate the FCC. Since mammals encode 13 aquaporins that exhibit tissue-selective expression [11], we first validate the aquaporin isoform(s) in brown adipocytes responsible for glycerol efflux. Next, we aim to translate intracellular glycerol accumulation to FCC activity by examining oxygen consumption rates and whole-body energy expenditure.

Overall, this project strives to provide new insight into the regulatory role of glycerol in thermogenesis and determine if thermogenesis by the FCC can be hyperactivated. Secondly, in the context of metabolic health, brown adipocyte-specific aquaporin isoform(s) could be a potential novel therapeutic target to amplify the protective role of the FCC against obesity [2,6,7].

RESULTS

[1]*Glycerol is an allosteric activator of TNAP and accelerates futile creatine cycling*

TNAP has been shown to significantly contribute to noradrenaline (NA) stimulated thermogenesis in brown adipocytes [9]. Since acute activation of thermogenesis triggers lipolysis, yielding glycerol and free fatty acids, it was hypothesized that lipid mobilization plays a role in TNAP activity (**Fig. 1A**). To test this, Hussain *et al.* developed an *in vitro* assay to study inducible futile creatine cycling. The assay combined mitochondrial or whole-cell lysate with pyruvate kinase (PK), lactate dehydrogenase (LDH), and corresponding substrates to establish an enzyme-coupled reaction (**Fig. 1B**). More specifically, the lysate contained both CKB and TNAP localized in mitochondria [8, 9]. ATP was added, allowing CKB to catalyze the phosphoryl transfer to creatine (Cr) and generate phosphocreatine (PCr) for TNAP. Phosphoenolpyruvate (PEP) was also added, enabling PK to catalyze the phosphoryl transfer to liberated ADP and replenish the ATP pool for CKB. Lastly, LDH used the pyruvate from PEP dephosphorylation to couple the oxidation of added NADH. Total futile creatine cycle (FCC) activity was measured as a readout of NADH oxidation.

Having validated the assay, FCC activity was measured in protease-protected brown adipose tissue (BAT) mitochondrial lysates in the presence of lipolytic products: palmitate (i.e. FFA) and glycerol. The reaction mix was supplemented with Cr or PCr to initiate cycling. If palmitate or glycerol stimulates the FCC via TNAP, a specific quantity of Cr or PCr would elicit a molar excess of NADH oxidation since ADP liberation and NADH oxidation are stoichiometrically equal. While palmitate had no stimulatory effect, glycerol accelerated the hydrolytic activity of TNAP and futile creatine cycling. Without glycerol, successful cycling only occurred when Cr was supplemented. PCr without glycerol was not sufficient to cause coupled NADH oxidation. However, when glycerol was supplemented with PCr, FCC activity via TNAP was stimulated, and NADH oxidation was

[1] Please note that figures corresponding to this results subsection were not included in the appendix for copyright reasons. The authors cannot confirm which journal the paper will be accepted in, so copyright approval could not be obtained from the corresponding publisher.

rescued. Furthermore, this property was BAT-specific, as protease-protected cardiac and hepatic mitochondria driven by PCr were not glycerol-inducible.

As previously established, due to the futile nature of creatine cycling each mole of Cr releases a super-stoichiometric quantity of ADP. Hussain *et al.* next aimed to observe the effect of glycerol-dependent acceleration of FCC activity on respiration and the stoichiometric relationship of Cr-dependent ADP liberation. To do so, respirometry was performed on freshly isolated BAT mitochondria. Mitochondria were supplemented with Cr and respiration was stimulated using ADP. Under control conditions, respiring mitochondria exhibited an approximately 1:18 stoichiometric relationship between Cr and ADP liberation. The addition of glycerol significantly amplified the super-stoichiometric quantity of ADP liberation to approximately 1:32. Collectively, these data suggested that glycerol amplifies FCC activity and drives thermogenesis in BAT via TNAP activation. However, the mechanism of action remained unclear.

During the hydrolysis of PCr to Cr, a phosphorenzyme forms where the inorganic phosphate (Pi) is temporarily bonded to the active site of TNAP [110]. Here Pi release from the enzyme complex is the rate-limiting step of PCr hydrolysis. Excitingly, in the presence of alcohol molecules such as glycerol (triol), the Pi can be released via a faster transphosphorylation reaction mechanism. Transphosphorylation reactions provide more than a 100-fold acceleration to the Pi release [110]. In the context of the FCC, Cr would be more readily available for CKB – expediting one of the rate-limiting factors of ADP liberation. To ascertain if glycerol behaves as the acceptor substrate of transphosphorylation, ^{31}P nuclear magnetic resonance was performed to observe PCr hydrolysis in the presence of glycerol across a 30 minute reaction. As expected, PCr peaks decreased over time. Surprisingly, inorganic phosphate release was much more prevalent compared to a minute increase in glycerol phosphate. This suggested that the mechanism of TNAP activation was not through a rapid phosphotransfer to glycerol but rather another form of enzymatic regulation.

To further explore how glycerol affects TNAP activity without partaking in the reaction, Hussain *et al.* visualized the novel crystal structure of murine TNAP. Encouragingly, both PCr and glycerol were found bound to the structure at 2.3 Å resolution. Using structure-function approaches, Hussain *et al.* identified a glycerol

binding pocket adjacent to TNAP's glycosylphosphatidylinositol (GPI) anchor. Additional assays outside the scope of this thesis validated that glycerol allosterically activated TNAP hydrolytic activity.

Together, these data identified a physiologically relevant regulator of TNAP that activates UCP1-independent thermogenesis and established the rationale for this present study. We aimed to harness this mechanism as a tool for facultative FCC activation by preventing glycerol export from brown adipocytes.

Aqp7 is the most abundant aquaporin isoform in brown adipocytes

13 aquaporin (Aqp) homologs have been identified in mammals that are variably expressed across cell types in tissues and organs [121]. To comprehensively detect all Aqps expressed in brown adipocytes, we mined ribosome profiling datasets [132] to score relative Aqp mRNA expression in adipose tissue. These datasets used translating ribosome affinity purification (TRAP) technology to genetically tag and selectively isolate polysomes from Adiponectin (AdipoQ) and UCP1 expressing cells from highly heterogenous adipose tissue. AdipoQ is highly adipose-specific and constitutively expressed in all mature adipocytes, while UCP1 is solely expressed in beige and brown adipocytes [133]. Relative mRNA expression of the 11 Aqp isoforms expressed in murine tissues was compared between whole adipose tissue and whole mouse tissue. We identified aquaporin 7 (Aqp7) as the most abundant glycerol transporter in BAT (**Fig. 2A**). In addition, Aqp7 was most prevalent in both inguinal and epididymal white adipose tissue (WAT). Intriguingly, relative Aqp7 mRNA was higher in beige adipocytes in WAT depots compared to brown adipocytes in BAT (**Fig. 2B**). Aqp11 exhibited a similar trend in thermogenic adipocytes, albeit at lower levels than Aqp7.

To independently validate these data, we assessed Aqp mRNA expression at various time points throughout brown adipocyte differentiation using RT-qPCR (**Fig. 2C**). Samples were harvested every 48 h from immortalized murine preadipocytes on day 0 to fully differentiated brown adipocytes on day 6. Relative mRNA expression of well-established adipogenic biomarkers [134]: peroxisome proliferator-activated receptor γ 2 (*Pparg2*), fatty acid-binding protein 4 (*Fabp4*), and *Ucp1* increased throughout and

verified successful differentiation (**Fig. 2D**). Here we confirmed Aqp7 as the most abundant transporter that increased in expression during differentiation at the mRNA and protein level (**Fig. 2E & 2F**). Aqp3 and Aqp11 were also induced during differentiation, but their levels were significantly lower than Aqp7 (**Fig. 2E**). Relative mRNA expression of other Aqps was not sustained in mature brown adipocytes (**Fig. 2G**). Overall, these data prompted us to focus on a shortlist of three candidate transporters: Aqp3, Aqp7, and Aqp11 – with an emphasis on Aqp7.

Thermogenic profiles of Aqp 3, 7 and 11

Glycerol plays a critical role in metabolic flexibility and is an intermediate for both lipid and glucose metabolism. Although glycerol serves as a substrate in thermogenesis, the thermogenic regulation of Aqps that mediate glycerol transport in BAT has not been examined. To gain better insight into the thermoregulation of our Aqp candidates, we explored how they are physiologically regulated during facultative thermogenesis. Wild-type (WT; C57BL/6N) mice were first acclimated to thermoneutral (TN) conditions (30°C) to equilibrate thermogenic machinery and then transferred to the cold (4°C or 6°C) for various times. RT-qPCR was subsequently performed on BAT. Interestingly, acute cold exposure for 60 min significantly increased Aqp7 mRNA, while Aqp3 mRNA increased only after 24 hr in the cold (**Fig. 3A & 3B**). Aqp11 was not cold-inducible (**Fig. 3A & 3B**), unlike canonical thermogenic effectors: UCP1, CKB, and TNAP, which increase in response to cold [19]. We also probed how our Aqp hits respond to chronic cold exposure when adaptive thermogenesis substitutes. Here only Aqp3 was cold-inducible for prolonged periods (**Fig. 3C**). Overall, Aqp3 was cold-induced under all tested conditions, Aqp7 was only acutely cold-induced, whereas Aqp11 was not regulated by environmental temperature.

Exposure to cold stimulates both α- and β-adrenergic receptors which synergistically trigger cold-induced thermogenesis downstream [63, 64]. Thus, we sought to distinguish the independent contributions of α- and β-adrenergic receptor signalling on Aqp candidates' mRNA expression. We probed the contributions of β-adrenergic receptors using pharmacological activation of ADRβ3 by CL 316,243 (CL). Under TN

conditions when thermogenic pathways are inactive, thermogenesis in WT mice was activated via bidaily intraperitoneal (i.p.) injections of CL over 54 hr. RT-qPCR analysis on BAT revealed increased Aqp3 mRNA abundance in response to CL relative to TN saline controls (**Fig. 3D**). Furthermore, ADRβ3 activation significantly decreased Aqp7 expression with no effects on Aqp11 relative to control (**Fig. 3D**). Next, we probed the contributions of α-adrenergic receptors. We mined a BAT RNA-seq dataset from mice pretreated with a single i.p. injection of either the α-AR antagonist phenoxybenzamine (PBZ) or saline control and then housed at 30 °C or 6 °C for 24 hr [82]. Rahbani *et al.* categorized the BAT transcriptome into four differentially expressed clusters of genes. Intriguingly, *Aqp3* was grouped alongside thermogenic FCC effectors *Ckb* and *Alpl* in the cluster of cold-induced genes repressed by PBZ treatment (**Fig. 3E**). Brown adipocyte *Ckb* and *Alpl* transcription in response to cold was shown to be controlled by complementary early B cell factors 1 & 2 (*Ebf1*/*Ebf2* encoding EBF1/EBF2) and peroxisome proliferator-activated receptor gamma co-activator 1 alpha (*Ppargc1a* encoding PGC1α) [82]. However, unlike *Alpl*, cold-inducible properties of *Ckb* were shown to be dependent on complementary estrogen-related receptors α & γ (Errα/Errg encoding ERRα/ERRγ) [82]. PGC1α is a well-established master transcriptional regulator that enhances energy production in response to cold and maintains metabolic homeostasis [135]. Additionally, PGC1α can function as a co-activator for ERRα or ERRγ – enabling coordinated control of the cold response [136]. Their cooperative action and binding on target thermogenic genes are facilitated by EBF2 [137]. Due to the mutual clustering of *Aqp3* with *Ckb* and *Alpl,* we hypothesized that *Aqp3* may be controlled under a similar model of transcriptional regulation. To elucidate if ERR, EBF, and PGC1α regulated our Aqp candidates, we respectively employed adipocyte-selective double knockout (DKO) mouse models of ERRα/ERRγ, EBF1/EBF2, and a brown adipocyte-selective inducible knockout (iKO mouse model of PGC1α. As before, WT and KO were first acclimated to TN conditions (30°C) to equilibrate thermogenic machinery and then transferred to the cold (4°C or 6°C) for 24 hr. Remarkably, the deletion of ERR, EBF, and PGC1α significantly ablated the cold-stimulated induction of *Aqp3* mRNA relative to WT control mice (**Fig. 3F**). Under non-acute conditions of cold exposure, Aqp7 mRNA was not consistently induced, and transcriptional machinery was dispensable towards overall

expression relative to WT and TN control mice (**Fig. 3G**). Surprisingly, Aqp11 exhibited an opposite trend regarding transcriptional control compared to Aqp3. More specifically, ERR, EBF, and PGC1α had inhibitory effects on Aqp11 expression under TN conditions. PGC1α deletion significantly induced Aqp11 mRNA expression that was dampened in response to cold. This trend was also observed in the EBF1/EBF2 DKO model. In the absence of ERRα/ERRγ, Aqp11 was transformed into a cold-induced gene (**Fig. 3H**). Altogether our findings show that Aqp3 can be induced by cold and is regulated by thermogenic the transcription factors we probed. While Aqp7 can be rapidly induced by cold, it is not regulated by the same thermogenic transcription factors. Lastly, Aqp11 is not induced by cold, but it is controlled by the same thermogenic transcription factors we investigated in an antithetical fashion to Aqp3.

Establishing and validating stable CRISPR/Cas9 knockout cell lines

To delineate the key aquaporin(s) regulating glycerol export from our shortlist, we endeavoured to generate stable knockout (KO) cell lines for AQP3, AQP7, and AQP11 in immortalized brown adipocytes using clustered regularly interspaced short palindromic repeats (CRISPR) technology (**Fig. 4A**). We selected a KO approach to eliminate any confounding effects from residual protein expression. The relative contribution of each Aqp to total glycerol export could be attributed. Stable KOs would also minimize glycerol leak and maximize available intracellular glycerol compared to alternative knockdown (KD) methods. We began with AQP7 since its expression levels in brown adipocytes were orders of magnitude greater than AQP3 and AQP11 (**Fig. 2E & 2F**). In brief, we engineered lentiviral constructs expressing three distinct single guide RNAs (sgRNAs) against Aqp7. An empty lentiviral vector served as the negative control. Preadipocytes were infected and selected for puromycin resistance. Successfully infected preadipocytes were then fully differentiated until day 6 before we confirmed KOs via western blot. However, none of the three cell lines (sgAqp7.1, .2, and .3) demonstrated KOs at the protein level relative to the vehicle control (**Fig. 4B**). Conversely, all sgRNA lines stably expressed flag-tagged CRISPR-associated protein 9 (Cas9), absent in uninfected mature brown adipocytes (**Fig. 4C**). Next-generation sequencing confirmed the successful

cloning of sgRNAs into the lentiCRISPRv2 backbone. Additionally, all infected cell lines were also puromycin-resistant throughout differentiation. We noticed a small decrease in the AQP7 signal in the sgAqp7.2 pool population. We thus decided to perform limiting dilutions to potentially isolate individual clones that exhibit a KO phenotype (**Fig. 4B**). A total of 18 clones were isolated and fully differentiated until day 6 before KO validation via western blot as previously done. Unfortunately, no clones were successful AQP7 KOs, despite all else indicating successful infection and selection (**Fig. 4D**). As a result, we did not pursue this technology for AQP3 and AQP11. Instead, we explored other techniques to manipulate Aqp-dependent glycerol export genetically.

Silencing Aqp7 in brown adipocytes diminishes glycerol release upon noradrenaline-stimulated lipolysis

Next, we determined the suitability of small interfering RNA (siRNA) technology for Aqp loss of function in mature brown adipocytes. Fully differentiated adipocytes are among the cell types most difficult to transfect due to their abundance of multilocular lipid droplets [138]. However, a reverse transfection method early in the adipocyte differentiation process has been shown to efficiently silence gene expression in mature brown adipocytes [124]. Thus, we reverse-transfected immortalized mouse brown adipocytes on day 3 of differentiation with a pool of four distinct Aqp7-specific siRNAs and continued differentiation until day 7. RT-qPCR and western blot validation revealed successful KD of Aqp7 at mRNA and protein levels relative to siScramble control (**Fig. 5A**). *Aqp7* silencing did not have any off-target effects on *Aqp3* and *Aqp11* isoforms. Furthermore, *Aqp7* KD did not influence adipocyte differentiation as mRNA expression levels of adipogenic markers (*Ucp1, Pparg1, Pparg2,* and *Pgc1a*) were not significantly altered. However, there were small opposing fluctuations in FCC effectors (*Ckb* and *Alpl* encoding TNAP) (**Fig. 5B**).

Once we established a system to examine Aqp7 loss of function, we performed glycerol release assays to quantify intra- and extra-cellular levels of glycerol following NA-stimulated lipolysis. Following NA treatment, we observed a significant decrease in glycerol efflux concomitant with an increase in intracellular glycerol in Aqp7 deficient

mature brown adipocytes. Interestingly, this trend was also represented under basal conditions void of adrenergic activation (**Fig. 5C**). We also tested the efficacy of pharmacological inhibition of Aqp7 using Z433927330, a potent and selective inhibitor of AQP7, which less potently inhibits AQP3 and AQP9 [139]. Z433927330 exhibited a dose-dependent decrease in extra-cellular glycerol levels during lipolysis (**Fig. 5D**). However, despite its affinity for AQP7, AQP3, and AQP9 (not expressed in adipocytes), siRNA-mediated KD proved to be more efficacious than pharmacological inhibition in preventing glycerol leak. Overall, a ~75% ablation in Aqp7 expression was responsible for a ~33% reduction in glycerol export compared to control conditions via siRNA-mediated KD (**Fig. 5A**). Therefore, genetic manipulation of Aqp7 successfully trapped glycerol within brown adipocytes.

Intracellular glycerol accumulation dampens thermogenesis by noradrenaline

To ascertain if the intracellular accumulation of glycerol translates to increased FCC activity, we investigated NA-stimulated brown adipocyte respiration using Seahorse bioanalyzer. First, we reverse-transfected differentiating brown adipocytes with a pool of Aqp7-specific siRNAs or scrambled control siRNA. To elucidate if trapping glycerol intracellularly increased thermogenesis in brown adipocytes, we observed oxygen consumption rates (OCR) as a readout of thermogenic capacity (**Fig. 6A**). Basal respiration rates, which are principally controlled by ATP turnover, were not impacted despite more available glycerol for cellular processes. Unexpectedly, we found that silencing of Aqp7 specifically decreased NA-stimulated respiration. More specifically, the absolute O_2 levels used to calculate OCR drop in a gradual, linear fashion and are not consumed immediately (**Fig. 6B**). Additionally, absolute O_2 levels fully recovered before the next measurements. Thus, the abrogation of the respiratory response observed during thermogenesis relative to the control was not due to complete oxygen depletion but rather metabolic effects. Next, no differences were observed in NA-dependent proton leak resulting from the inhibition of mitochondrial ATP synthase by oligomycin. Additionally, maximal respiration mediated by 2,4-dinitrophenol (DNP) uncoupling of the electron transport chain (ETC) was significantly decreased by trapped glycerol. Lastly,

inhibition of mitochondrial complex I and complex III of the ETC using rotenone and antimycin A respectively, had no discernible effects on OCR. Extracellular acidification rate (ECAR) data were not included since it is not a suitable measure of glycolytic flux of adipocytes during active lipolysis initiated by NA [125]. These data suggest that glycerol accumulating within brown adipocytes during lipolysis causes respiratory defects in the form of NA-stimulated thermogenesis and maximal respiratory capacities.

Having determined the respiratory consequences of glycerol accumulation through impeded glycerol export, we sought to investigate the thermogenic effects of glycerol accumulation through excess glycerol import *ex vivo*. We freshly isolated mature brown adipocytes from WT mice and subjected them to an oxygen electrode in a glycerol-free respiration buffer to quantify OCR in response to glycerol and NA. After an initial basal OCR, glycerol was introduced in excess at 1 mM or 10 mM. These extracellular concentrations exceeded intracellular levels of glycerol to ensure entry via facilitated diffusion. Additionally, 1 mM of glycerol was used by Hussain *et al.* to observe the aforementioned super-stoichiometric effects of glycerol on FCC activity. While basal OCRs were consistent between all groups as expected, glycerol concentration was negatively correlated with glycerol-dependent OCR (**Fig. 6C & 6D**). Furthermore, upon NA stimulation, the presence of glycerol significantly abrogated the thermogenic response (**Fig. 6E**), similar to what was seen *in vitro* (**Fig. 6A**). Representative traces encapsulate how the presence of glycerol significantly diminished O_2 consumption and overall thermogenic capacity of mature brown adipocytes (**Fig. 6F**). These data were consistent with our Seahorse data wherein intracellular accumulation of glycerol strongly impaired NA-stimulated respiration. Both experiments independently refuted our hypothesis as we expected readily available glycerol to allosterically activate more TNAP units, increase PCr hydrolysis and FCC-mediated ATP turnover, and in turn, elevate oxygen consumption.

Fat-specific silencing of Aqp7 in vivo reduces whole-body energy expenditure

Despite unsuccessful attempts to employ genetic ablation to rapidly activate the FCC and increase brown adipocyte respiration *in vitro* and *ex vivo*, we probed our hypothesis *in*

vivo. Recapitulating the physiological environment and considering complex cellular interactions *in vivo* have been shown to identify unique genetic dependencies left uncovered by *in vitro* models [140]. Previous studies have used germline Aqp deletion mouse models [119, 121, 122]; however, since aquaporins are expressed in various tissues, the role of aquaporins in brown adipocytes remains elusive. To address this, we silenced Aqp7 *in vivo* by infecting Adipoq-Cre mice that selectively express cre-recombinase in adipocytes with cre-inducible short hairpin RNAs (shRNAs) packaged in adeno-associated virus (AAV) vectors [130]. Recombinant AAVs were surgically injected into interscapular BAT (iBAT). Mice recovered for 2 weeks post-op to allow ample time for cre-recombinase activity (**Fig. 7A**). Using RT-qPCR we confirmed the efficacy of two distinct constructs in downregulating Aqp7 expression relative to shLacZ control (**Fig. 7B**). Similar to siRNA-mediated silencing, successful KD of Aqp7 did not have off-target effects on *Aqp3* and *Aqp11* isoforms (**Fig. 7C**). Moreover, decreased glycerol export under basal conditions from BAT did not affect glycerol kinase (*Gyk*) expression. Fascinatingly, silencing of Aqp7 *in vivo* increased *Ckb* and decreased *Alpl* expression in both males and females – similar to siRNA-mediated KD *in vitro*. Next, we investigated the role of Aqp7 on whole-body energy expenditure (EE) using indirect calorimetry. We tested both males and females to control for previously identified sexual dimorphism in BAT activation [141]. Experimental groups were weight-matched to ensure discrepancies in EE were not confounded by body mass variability (**Fig. 7D**). We administered subcutaneous injections of NA above the iBAT to anesthetized mice to pharmacologically activated EE. Both male and female mice deficient in Aqp7 exhibited similar reductions in EE elicited by NA compared to controls (**Fig. 7E & 7F**). Altogether, these data point towards an unknown mechanism through which Aqp7 increases EE.

DISCUSSION & CONCLUSION

Obesity has become a significant public health concern in recent decades. Identifying therapeutic approaches to combat this global epidemic is of utmost importance to lower the economic burden and decrease the rates of associated comorbidities. BAT and its thermogenic properties provide a physiological mechanism that can be targeted to increase daily EE. Longitudinal increases in EE significantly ameliorate the chronic energy imbalance observed in obese individuals. Currently, the BAT field is elucidating its underlying regulatory mechanisms. Pathways that activate or inhibit BAT NST present novel targets to potentially combat obesity. For example, a recent study identified that elevated succinate levels drove activation of thermogenesis and provided protective effects against DIT [142]. This opens the door to delivering succinate-based dietary supplements to promote weight loss. This is just one of the many recent studies that have sought to identify novel anti-obesity therapeutic approaches, and our work contributes to these efforts by investigating the potential therapeutic implications of glycerol as an allosteric activator of TNAP in the FCC.

In an effort to identify the underlying mechanisms of UCP1-independent thermogenesis, the Kazak group identified glycerol as an allosteric activator of TNAP using a series of structure-function approaches, bioenergetics, and cell biology. This opened the door to investigate the regulatory role of glycerol in thermogenesis. Preventing glycerol export from brown adipocytes will increase its binding efficiency to TNAP and may provide a method to hyperactivate the FCC through enhanced TNAP catalytic activity.

The most abundant source of glycerol within brown adipocytes is derived from the hydrolysis of TAG stores. When glycerol accumulates, it is exported out by a subset of aquaporins, called aquaglyceroporins, through facilitated diffusion. Past studies have identified that the likely aquaglyceroporin in adipose tissue is the Aqp7 isoform. However, it remained unclear if it was generic to all adipose tissue or specific to only WAT, especially considering how BAT and WAT are known to have intrinsic differences in genetic signatures. Here we provide further insight into the role of Aqp7 in brown adipose tissue. By mining ribosome profiling data and tracking the expression of all mammalian

aquaporin isoforms during brown adipocyte differentiation, we independently validated Aqp7 as the most abundant aquaporin isoform in BAT (**Fig. 2A-2C**). Intriguingly, relative Aqp7 mRNA was higher in UCP1^{+} beige adipocytes from WAT depots compared to brown adipocytes in BAT (**Fig. 2B**). This highlights a potential role of Aqp7 overexpression in promoting 'browning,' a phenomenon where white adipocytes develop brown adipocyte characteristics. In addition to Aqp7, these data highlighted a potential role of Aqp3 and Aqp11 in brown adipocytes, although their expression levels were orders of magnitude lower than Aqp7. Furthermore, Aqp3 and Aqp7 have similar levels of glycerol permeability [114]. Therefore, it is not that Aqp3 is far more permeable to glycerol and thus does not need to be as abundantly expressed. Research on Aqp3 has grown exponentially in the last decade and has been linked to the PI3K/AKT pathway involved in the secretion of proinflammatory cytokines [143]. Although obesity is heavily linked with inflammation, Aqp3 has not been investigated in the context of adipose tissue. Unlike the rising interest in Aqp3, little is known about Aqp11, primarily linked to renal diseases [144]. Encouragingly, both Aqp3 and Aqp11 have been posited as members of the aquaglyceroporin subset. Therefore, we decided to include them in our aquaporin 'candidate' list and investigate their involvement in glycerol transport in BAT. A potential next step could be performing a proximity-dependent biotinylation labelling technique (TurboID) of Aqp3, 7, and 11. TurboID analysis allows the monitoring of proximal/transient interactions of the protein of interest. This would enable us to establish the interactome of each aquaporin in the presence and absence of thermogenic stimuli (i.e. cold or pharmacological) to identify both canonical and non-canonical mechanisms in BAT.

Secondly, our cold exposure experiments identified the cold-inducible properties of Aqp3 and Aqp7 and some insight regarding how they are transcriptionally regulated in BAT. Our data indicates that Aqp7 is only acutely cold-inducible and not under chronic conditions (**Fig. 3A-3C**). Under acute conditions, facultative thermogenesis is activated, and lipolysis is triggered, leading to a build-up of intracellular glycerol. The FFAs would be used to drive NST, but this would trigger an upregulation of Aqp7 to prevent excessive buildup of glycerol. However, under chronic conditions, BAT would be highly active and therefore require all the macronutrients at its disposal to ensure it can maintain the metabolic flux associated with thermogenesis. In addition, one would expect the TAG

stores in brown adipocytes to be depleted after multiple days of cold exposure, thus removing the need for Aqp upregulation. While Aqp7 follows this train of thought, Aqp3 is cold-inducible under chronic and not acute conditions (**Fig. 3A-3C**), further highlighting the potential non-canonical role Aqp3 may play in brown adipocytes. Performing these cold-exposure experiments in Aqp7 deficient models could provide further insight regarding the role of Aqp3 and whether it has any compensatory effects in the absence of Aqp7.

Our observation of Aqp expression following adrenergic stimulation revealed some contradictory results. Activation of ADRβ3 increased Aqp3 expression, suggesting that it is linked to the Gs pathway (**Fig. 3D**). However, when we observe the RNA-Seq data from Rahbani *et al.* [82], treatment with PBZ, an α-AR antagonist, causes a decrease in Aqp3 expression (**Fig. 3E**). Therefore, blocking with Gq pathway during cold exposure abrogated the cold-inducible properties of Aqp3. It is important to note that these results are not conclusive but were instead performed to gain an understanding of how our aquaporin candidates behave in response to various thermogenic stimuli. One potential explanation for these results is that if an α-AR agonist (i.e. A61603) was combined with CL, an even more considerable increase in Aqp3 expression might be seen. Furthermore, the 6°C PBZ treatment appears to induce Aqp3 more than TN (30°C) conditions alone. Together, this highlights a potential synergic role of both Gs and Gq pathways in Aqp3 expression. Our proposed transcriptional model for Aqp3 shares key regulatory features seen in *Ckb* and *Alpl* transcriptional regulation, which are also linked to both Gs and Gq pathways. Although these RT-qPCR experiments linked Aqp3 and Aqp11 are linked to ERRα/ERRg, EBF1/EBF2, and PGC1α, unlike Aqp7 (**Fig. 3F-3H**), they are comprehension representations of their transcriptional control. This would entail performing ATAC sequencing coupled with CHIP sequencing to identify enriched transcriptional motifs proximal to Aqp3, 7, or 11. Furthermore, investigating their transcriptional control may reveal novel targets to potentially activate or inhibit these genes if they are linked to obesity. Keeping in mind the primary aim of this project is to determine if trapping of glycerol can hyperactivate the FCC, we used these experiments to shed some light on how our chosen Aqp candidates behave under thermogenic conditions. Overall, Aqp7 emerges as the primary candidate due to its outright abundance

in BAT. However, exploring Aqp3 has yielded intriguing observations regarding its regulation and potential non-canonically involvement in the thermogenic response.

Next, we validated CRISPR/Cas9 brown adipocyte cell lines for AQP7-KO before experimental use. Preadipocytes were infected with lentivirus containing lentiCRISPRv2 constructs expressing sgRNAs targeting AQP7 and were fully differentiated to induce Aqp7 before validation. Despite being puromycin-resistant and stably expressing Cas9, none of the isolated clones were AQP7-KO (**Fig. 4C & 4D**). The brown preadipocytes were previously isolated from the stromal vascular fraction of BAT and immortalized in-house using simian virus 40 (SV40) virus large T-antigen (T-Ag). It has been shown that once cell lines harbour the integration of one lentiviral vector, subsequent lentiviral infections dramatically lose their efficacy [145, 146]. This seems the most probable explanation to explain why we were unable to establish stable Aqp7-KOs despite all else indicating successful integration. We employed CRISPR/Cas9 before other KD techniques to minimize glycerol leaks. In addition, since we did not know the relative contributions of Aqp3, 7, & 11 towards glycerol transport in brown adipocytes, we felt a KO model would allow us to attribute the specific roles of each isoform. After being unsuccessful with the lentiCRISPRv2 system, we sought to use siRNA- and shRNA-mediated KD *in vitro* and *in vivo,* respectively (**Fig. 5A & 7B**). A KD approach came with its own set of advantages. Glycerol import is essential for normal adipocyte function. Therefore, deleting aquaporins may be detrimental to cells and not recapitulate physiological conditions. In addition, there is always the possibility that compensatory effects take over where other Aqp isoforms take over for Aqp7 and misrepresent results once again. With a KD, we overcame these drawbacks of the lentiCRISPRv2 system and successfully decreased Aqp7 expression in both fully differentiated brown adipocytes and BAT (**Fig. 5A & 7B**). These methods provided *in vitro* and *in vivo* model systems for downstream experiments.

Depleting Aqp7 significantly decreased the amount of glycerol released into the extracellular space. In parallel, we observed an increase in the intracellular glycerol concentrations (**Fig. 5C**). This also complied with literature in which global AQP7-KOs had decreased plasma glycerol levels [122] – similar to what we observed under basal conditions. Pharmacological inhibitions of AQP7 using Z433927330, a potent and

selective inhibitor, also resulted in a decrease in glycerol export, but these effects were observed well beyond the published IC_{50} of 0.2 μM (**Fig. 5D**). Due to the potentially toxic doses required to ablate glycerol export significantly, we proceeded with genetic manipulation. Overall, the glycerol release assay served its purpose as we successfully identified the aquaporin isoform in brown adipocytes responsible for glycerol efflux in support of our hypothesis.

Finally, from our *in vitro* and *ex vivo* respirometry experiments, we could not translate the intracellular trapping of glycerol to increased cellular respiration and oxygen consumption. If we had observed an increase in OCR, the next step would have been to determine if it was a TNAP-dependent increase. However, in direct contradiction to our hypothesis, the accumulation of glycerol within brown adipocytes significantly reduced NA-stimulated respiration (**Fig. 6**). From our Seahorse experiments, the Levels data showed shallow drops in consumed oxygen during NA-stimulation (**Fig. 6B**) coupled with a decrease in maximal respiration during DNP treatments (**Fig. 6A**). Together, these data portray some form of metabolic defect occurs when Aqp7 is inhibited. During NA stimulation, lipolysis occurs and releases FFAs and glycerol. The FFAs can be used for substrate oxidation to drive respiration, but glycerol accumulates. We hypothesized that this would make it more readily available to bind to TNAP and accelerate the FCC. However, this is not the case. It is possible that glycerol accumulates to the point where it causes lipotoxicity. Lipotoxicity occurs when lipid levels reach toxic levels within tissues and has been linked to chronic adipose tissue inflammation and mitochondrial dysfunction [147]. Lipolysis is regulated by a multi-enzyme complex that exists and exists in a delicate balance. Therefore, if glycerol accumulates, the final step of lipolysis performed by MGL to release the final FFA and glycerol might not occur because glycerol is already so prevalent and monoglyceride accumulates. This could cause lipotoxicity within the cells and explain the decrease in OCRs we observed, along with the impaired maximal thermogenic capacity. Furthermore, in our respirometry assay with freshly isolated mature brown adipocytes, we see that higher glycerol levels have increased impairment of respiratory capacity (**Fig. 6D & 6E**). Glycerol-dependent OCR indicates the change in basal respiration in the presence of glycerol. NA-dependent OCR independently supports the Seahorse data and shows a significant drop in OCR with glycerol.

In our final set of experiments, fat-specific deletion of Aqp7 *in vivo* also had identical results following NA stimulation. Here, we observed a decrease in overall EE, which is representative of OCR (**Fig. 7E & 7F**). Altogether, there appears to be some unknown mechanism through which Aqp7 increases OCR and EE. Previous studies that used global Aqp7-KOs found that they were more susceptible to obesity [119, 120, 121]. This is in line with our data but refutes our hypothesis. These groups presented the rationale that glycerol accumulation in WAT stores promotes glycerol kinase activity and, ultimately, glycerol re-esterified into TAG stores. Therefore, these mice cannot hydrolyze TAG stores, which continue to accumulate and potentiate their obese characteristics. However, it is important to note that we did not observe an increase in relative mRNA expression of *Gyk* between control and shAqp7 groups (**Fig. 7C**) – although enzymatic activity could be elevated. Furthermore, the synthesis of TAG and incorporation into LDs would discredit the possibility of lipotoxicity because the monoglycerides would not accumulate. Another possible explanation is the brown adipocytes developing characteristics representative of white adipocytes, known as BAT 'whitening.' BAT whitening can be induced by various factors, including high temperatures, adrenergic signalling impairment, and lipase deficiency [148]. Inhibiting glycerol export is highly representative of lipase deficiency because lipolysis will not function properly on a systemic level. After all, glycerol is not released. Therefore, the brown adipocytes deficient in Aqp7 are more prone to TAG synthesis, a hallmark of white adipocytes and long-term storage; then, they could gradually undergo 'whitening' and lose their thermogenic capacity. This would explain the decreased EE observed *in vivo*. To test this new hypothesis, transcriptional profiles of BAT from Aqp7 deficient mice can be compared to WT mice exposed to cold. The cold-exposed group will have a robust thermogenic signature to which we can compare the Aqp7-null signature and determine if there is evidence of whitening and loss of thermogenic capacity. A combination of factors may be at play here, but Aqp7 appears strongly linked to obesity.

In conclusion, while we successfully identified the primary aquaporin isoform in BAT and prevented glycerol import, we were ultimately unable to harness the trapped glycerol to hyperactivate the FCC via increased TNAP activity. To begin, these experiments highlighted the regulatory role of glycerol in thermogenesis. Secondly, they

strongly supported the role of Aqp7 in obesity, but our data suggest that it is likely through a mechanism or activation rather than inhibition. Subsequent studies can follow a similar set of experiments to those performed in this project but with an overexpression approach instead of KO or KD. Some potential setups include determining the effects of overexpressing Aqp7 on 1) EE using indirect calorimetry, 2) protective effects against diet-induced thermogenesis, and 3) cold-sensitivity using chronic and acute cold exposure. Future studies can also investigate how to activate its transcription, translation, and activity physiologically. Overall, Aqp7 activation shows great promise as a target for combating obesity.

APPENDIX: TABLES

Table 2.0 – Primer sequences used for RT-qPCR.

Gene Name and ID	**Forward Primer**	**Reverse Primer**
Alpl (ID: 11647)	CCAACTCTTTTGTGCCAGAGA	GGCTACATTGGTGTTGAGCTTTT
Aqp1 (ID: 11826)	AGGCTTCAATTACCCACTGGA	GTGAGCACCGCTGATGTGA
Aqp11 (ID: 66333)	CTATGCAGGAGGGAGCCTCA	AAAGTGCAGAGAAAGTGCCAG
Aqp12 (ID: 208760)	CATCTGTGAGGTGGCTAGAAGG	AACACTCGCATCTCCAGGC
Aqp2 (ID: 11827)	ATGTGGGAACTCCGGTCCATA	ACGGCAATCTGGAGCACAG
Aqp3 (ID: 11828)	GCTTTTGGCTTCGCTGTCAC	TAGATGGGCAGCTTGATCCAG
Aqp4 (ID: 11829)	CTTTCTGGAAGGCAGTCTCAG	CCACACCGAGCAAAACAAAGAT
Aqp5 (ID: 11830)	AGAAGGAGGTGTGTTCAGTTGC	GCCAGAGTAATGGCCGGAT
Aqp6 (ID: 11831)	GTGTAGCAGGGCTTACCTTCT	GATGGCGATCTGGAGCACA
Aqp7 (ID: 11832)	AATATGGTGCGAGAGTTTCTGG	ACCCAAGTTGACACCGAGATA
Aqp8 (ID: 11833)	TGTGTAGTATGGACCTACCTGAG	ACCGATAGACATCCGATGAAGAT
Aqp9 (ID: 64008)	TGGTGTCTACCATGTTCCTCC	AACCAGAGTTGAGTCCGAGAG
Ckb (ID: 12709)	GCCTCACTCAGATCGAAACTC	GGCATGTGAGGATGTAGCCC
Cyclophilin (ID: 19035)	GGAGATGGCACAGGAGGAA	GCCCGTAGTGCTTCAGCTT
Fabp4 (ID: 11770)	AAGGTGAAGAGCATCATAACCCT	TCACGCCTTTCATAACACATTCC
Gyk (ID: 14933)	TGAACCTGAGGATTTGTCAGC	CCATGTGGAGTAACGGATTTCG
Pparg2 (ID: 19016)	TGCCTATGAGCACTTCACAAGAAAT	CGAAGTTGGTGGGCCAGAA
Pgc1a (ID: 19017)	TATGGAGTGACATAGAGTGTGCT	GTCGCTACACCACTTCAATCC
Ucp1 (ID: 22227)	AAGCTGTGCGATGTCCATGT	AAGCCACAAACCCTTTGAAAA

Table 3.0 – Single guide RNA (sgRNA) sequences ligated into lentiCRISPR v2 (Plasmid #52961) for lentivirus preparation are listed as follows.

Gene	**Sense**	**Antisense**
Aqp3_1	CACCGCAGTACACACACAATAAGGG	AAACCCCTTATTGTGTGTGTACTGC
Aqp3_2	CACCGACATTGCGAAGGTCACAGCG	AAACCGCTGTGACCTTCGCAATGTC
Aqp3_3	CACCGTATAACAACCCTGTGCCCCG	AAACCGGGGCACAGGGTTGTTATAC
Aqp7_1	CACCGTTCCTGAATACATGACACTG	AAACCAGTGTCATGTATTCAGGAAC
Aqp7_2	CACCGAGTCACTGCGGCATTCATGT	AAACACATGAATGCCGCAGTGACTC
Aqp7_3	CACCGACAAGGATGCCTATCACGAG	AAACCTCGTGATAGGCATCCTTGTC
Aqp11_1	CACCGCCCCCGAAATGGGTGCCGTG	AAACCACGGCACCCATTTCGGGGGC
Aqp11_2	CACCGGGCACAGCTAGCAACCCGTG	AAACCACGGGTTGCTAGCTGTGCCC
Aqp11_3	CACCGAGCTAGAAACTCCAGGACGA	AAACTCGTCCTGGAGTTTCTAGCTC

Table 4.0 – Small interfering RNA (siRNA) sequences used for reverse transfection. Note siAqp7 was a pooled siRNA treatment comprised of four different siRNAs.

Name	**Sequence**
Scramble	GGA GUG GCC CAA CCC UCA GTG
siAqp7_1	AGG CAU GAA CUC CGG AUAU
siAqp7_2	CCA UGU AGC AGG CGG CAUC
siAqp7_3	CAA UUG UGC ACU AGG CCGA
siAqp7_4	GGA UGA GGC AUU CGU GACU

Table 5.0 – Short hairpin RNA (shRNA) sequences ligated into pDIO-DSE-mCherry-PSE-MCS (Plasmid #129669) for Adeno-associated virus (AAV) preparation are listed as follows.

Gene Name	**Sense**	**Antisense**
Aqp7_1	CTAGCAGCTACCACCTACTTAATTTCCTGACCCAAAATTAAGTAGGTGGTAGCTGTTTTTG	AATTCAAAAACAGCTACCACCTACTTAATTTTGGGTCAGGAAATTAAGTAGGTGGTAGCTG
Aqp7_2	CTAGGACTACCCTGCTTGGCATATTCCCTGACCCAGAATATGCCAAGCAGGGTAGTTTTTTG	AATTCAAAAAACTACCCTGCTTGGCATATTCTGGGTCAGGGAATATGCCAAGCAGGGTAGTC

Aqp7_3	CTAGGTATTGTATACCTGGGTTTAATCCTGACCCAATTAAACCCAGGTATACAATATTTTTG	AATTCAAAAATATTGTATACCTGGGTTTAATTGGGTCAGGATTAAACCCAGGTATACAATAC
Aqp7_4	CTAGGCCTTGTGTATGCTAGGTAATCCTGACCCAATTACCTAGCATACACAAGGCTTTTTG	AATTCAAAAAGCCTTGTGTATGCTAGGTAATTGGGTCAGGATTACCTAGCATACACAAGGC
lacZ	CTAGGTCGGCTTACGGCGGTGATTTCCTGACCCAAAATCACCGCCGTAAGCCGACTTTTTG	AATTCAAAAAGTCGGCTTACGGCGGTGATTTTGGGTCAGGAAATCACCGCCGTAAGCCGAC

APPENDIX: FIGURES

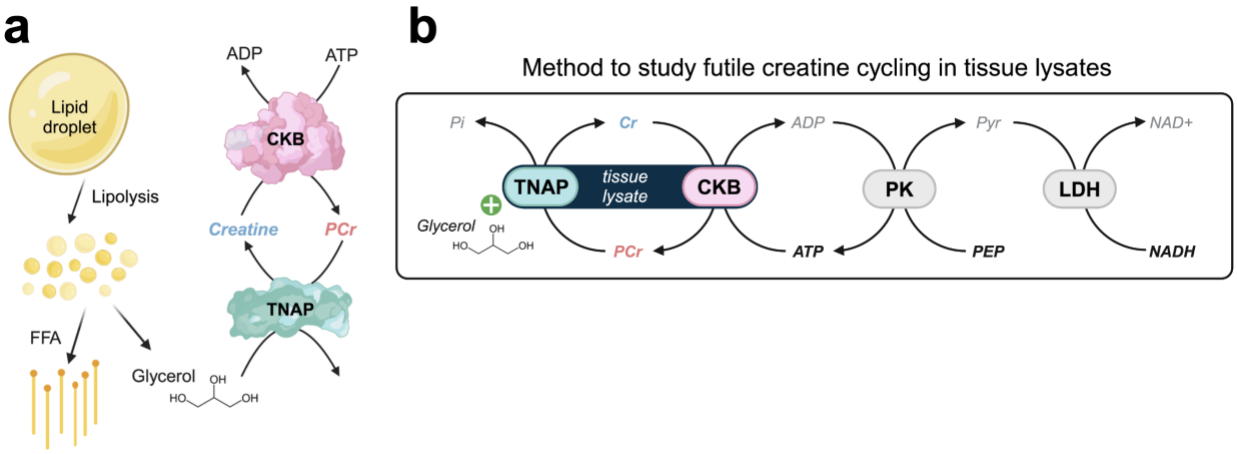

FIGURE 1. Lipid mobilization and the futile creatine cycle. (**A**) Schematic of the futile creatine cycle and physiological connection to glycerol. (**B**) Schematic of homemade enzyme-coupled reaction to test futile creatine cycling. Cr, creatine; PCr, phosphocreatine; CKB, creatine kinase b; TNAP, tissue non-specific alkaline phosphatase; Pi, inorganic phosphate; PK, pyruvate kinase; LDH, lactate dehydrogenase; ADP, adenosine diphosphate; ATP, Adenosine triphosphate; Pyr, pyruvate; PEP, phosphoenolpyruvate; NADH, Nicotinamide adenine dinucleotide. Created with BioRender.com

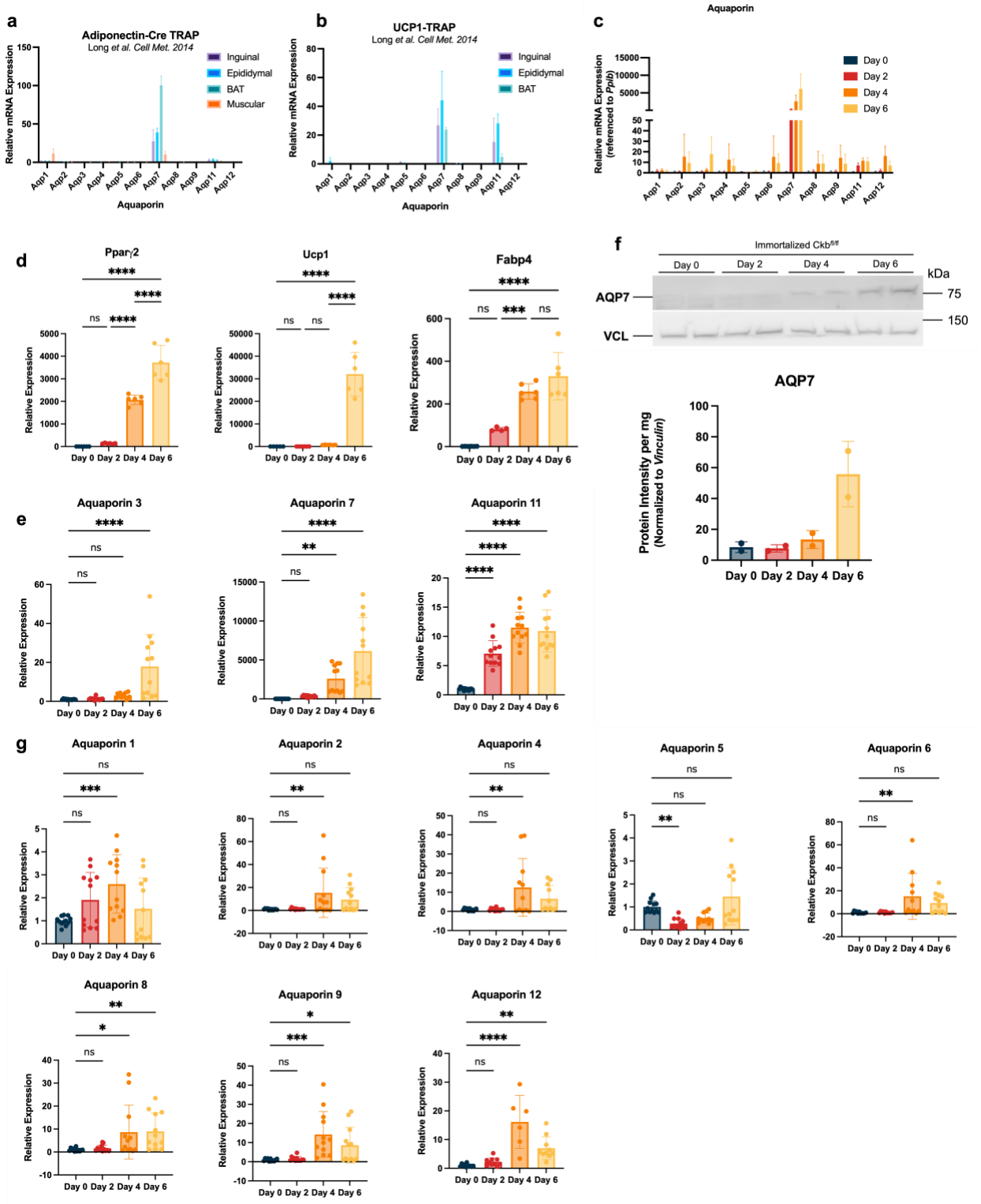

FIGURE 2. Aqp7 is the most abundant aquaporin isoform in brown adipocytes. (**A**) Ribosomal profiling from TRAP of AdipoQ+ adipocytes from different tissues in mice (n=3) [132]. mRNA expression in whole adipose tissue relative to whole mouse tissue. (**B**) Ribosomal profiling of Ucp1+ adipocytes (n=3). (**C**) RT-qPCR of murine aquaporin

isoform expression during brown adipocyte differentiation *in vitro* (n=6-12). (**D**) RT-qPCR of mature brown adipocyte markers during differentiation *in vitro* (n=4-6). (**E**) RT-qPCR of aquaporin isoforms that increase during differentiation. (**F**) Western blot and densitometry of AQP7 in brown adipocyte whole cell lysates during differentiation (n=2). (**G**) RT-qPCR of all aquaporins expressed in brown adipocytes during differentiation. One-way ANOVA (Fisher's LSD).

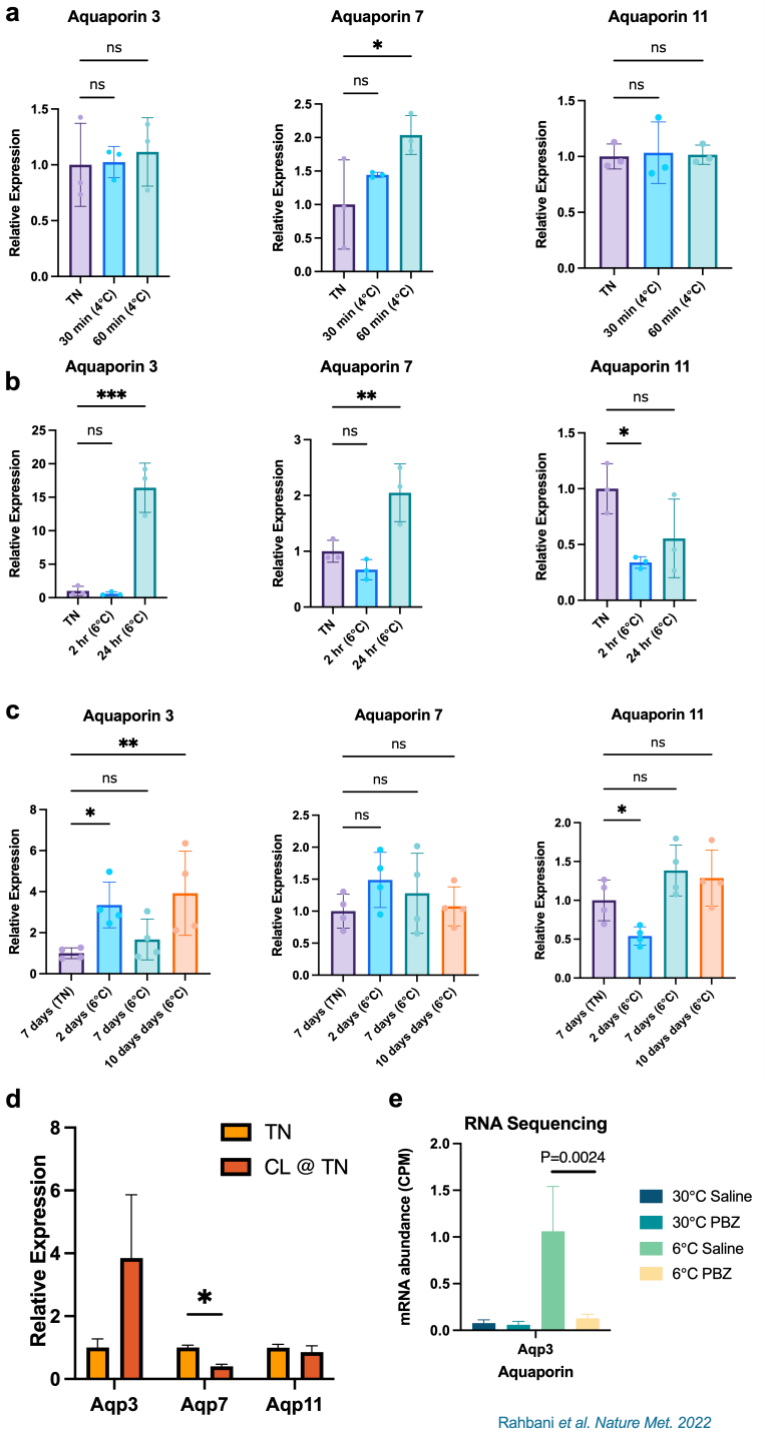

Rahbani *et al. Nature Met. 2022*

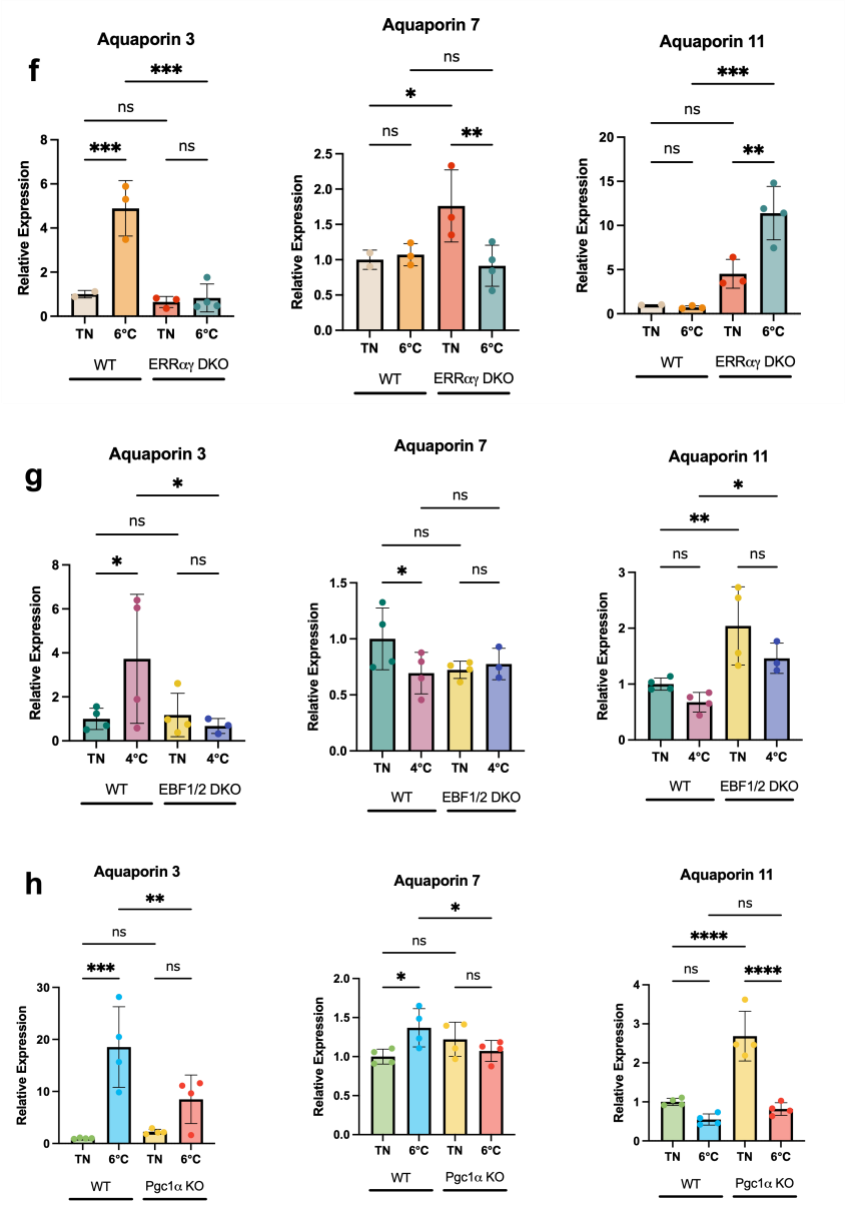

FIGURE 3. Thermogenic profiles of candidate aquaporins in brown adipose tissue. (**A**) RT-qPCR from BAT 60 minutes after 4°C cold exposure (n=3 per group, females). (**B**) RT-qPCR from BAT 24 hours after 6°C cold exposure (n=3 per group, females). (**C**) RT-qPCR from BAT during chronic cold-exposure at 6°C (n=4 per group, males). (**D**) RT-qPCR from BAT following bidaily CL 316,243 (CL) intraperitoneal injections under thermoneutral (TN, 30 °C) conditions after 54 hours (n=3 per group, females). (**E**) Aqp3 RNA sequencing following 24 h of 6 °C exposure and/or single intraperitoneal injection pan-α-AR antagonist phenoxybenzamine (PBZ) (n=3 per group, females) [82]. (**F**) RT–qPCR from BAT 24 h after 6 °C exposure (n = 2-3 per group, males). (**G**) RT–qPCR from BAT 7 days after 6 °C exposure (n = 3-4 per group, males). (**H**) RT–qPCR from BAT 48 h after 6 °C exposure (n = 4 per group, females). (**A-C**) One-way ANOVA (Fisher's LSD); (**D**) Two-tailed student's t-tests; (**E-H**) Two-way ANOVA (Fisher's LSD).

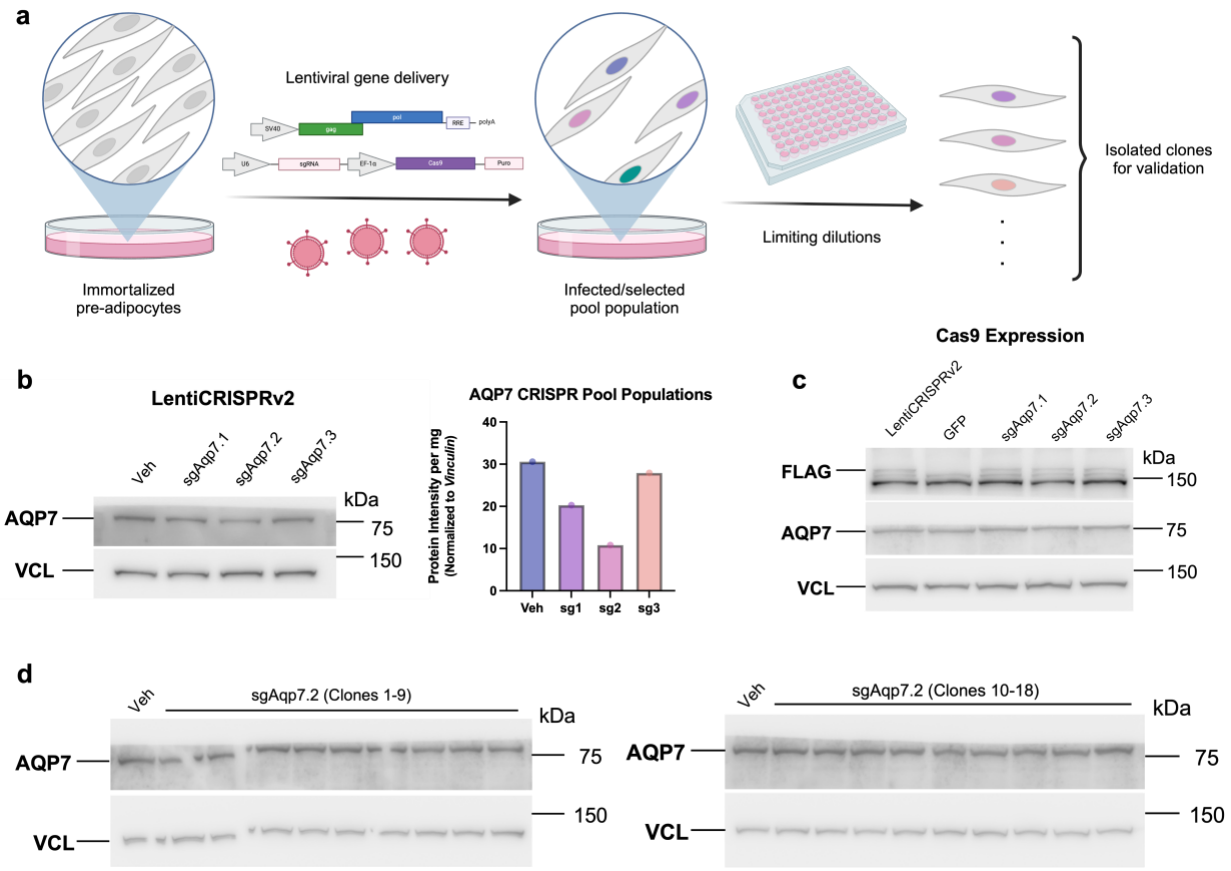

FIGURE 4. Establishing stable aquaporin KO brown preadipocyte cell lines for differentiation. (**A**) Overview of workflow for infection and selection of preadipocytes with recombinant lentivirus. Pool populations underwent subsequent limiting dilutions to isolate single clones devoid of AQP7. Created with BioRender.com (**B**) Western blot and densitometry analysis of puromycin-selected (i.e. positively infected) pool populations of differentiated brown adipocytes for KO validation. Veh, vehicle vector without sgRNA scaffold, expressing non-targeting Cas9. Three independent sgRNAs were designed to target various exons of the gene of interest. Densitometry was performed on ImageJ. (**C**) Western blot of differentiated brown adipocytes from infected pool populations validating Cas9 expression and viral integration into the host genome. LentiCRISPRv2, infected with empty lentiviral vector; GFP, uninfected mature brown adipocytes. (**D**) Western blots of 18 differentiated brown adipocyte clones selected from sgAqp7.2 pool population.

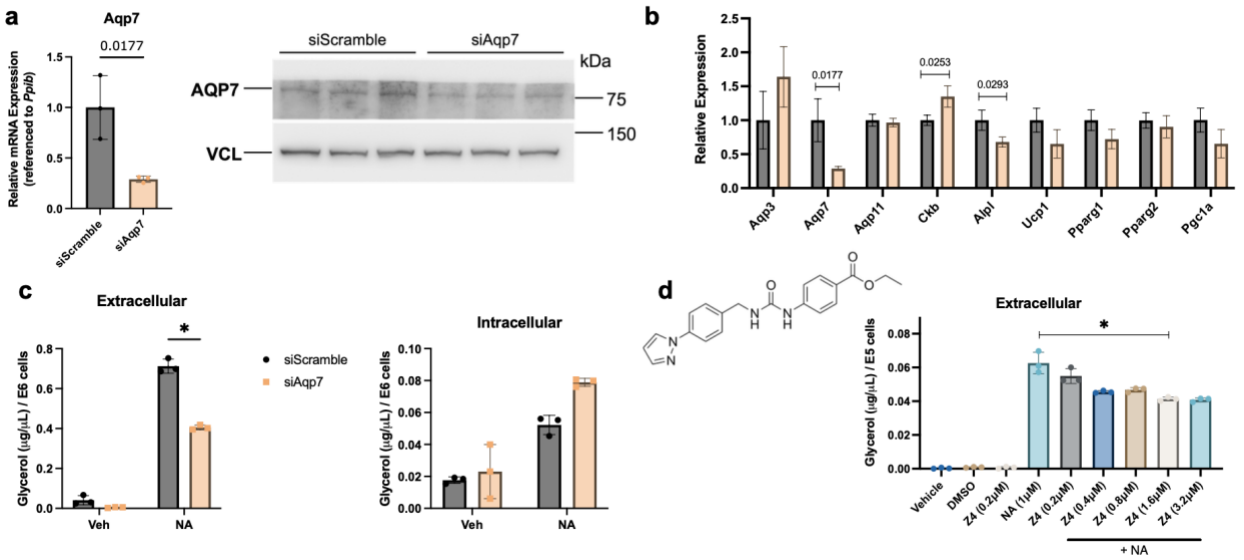

FIGURE 5. Aqp7 exports glycerol during noradrenaline-stimulated lipolysis in brown adipocytes. (**A**) Levels of Aqp7 following RNA interference in mature brown adipocytes using RT-qPCR and western blot (n=3). (**B**) RT-qPCR of adipogenic markers and Aqp isoforms in mature brown adipocytes following siRNA reverse transfection (n=3). (**C**) Glycerol release assay determining extracellular and intracellular levels of glycerol in mature brown adipocytes after Aqp7 KD under basal (Veh) and lipolytic conditions (NA) (n=3 per group). (**D**) Glycerol release in mature brown adipocytes following treatment with Aqp7 inhibitor, Z433927330, before NA-stimulated lipolysis (n=3). (**A-B**) Two-tailed student's t-tests (**C**) Two-way ANOVA (Fisher's LSD); (**D**) One-way ANOVA (Fisher's LSD).

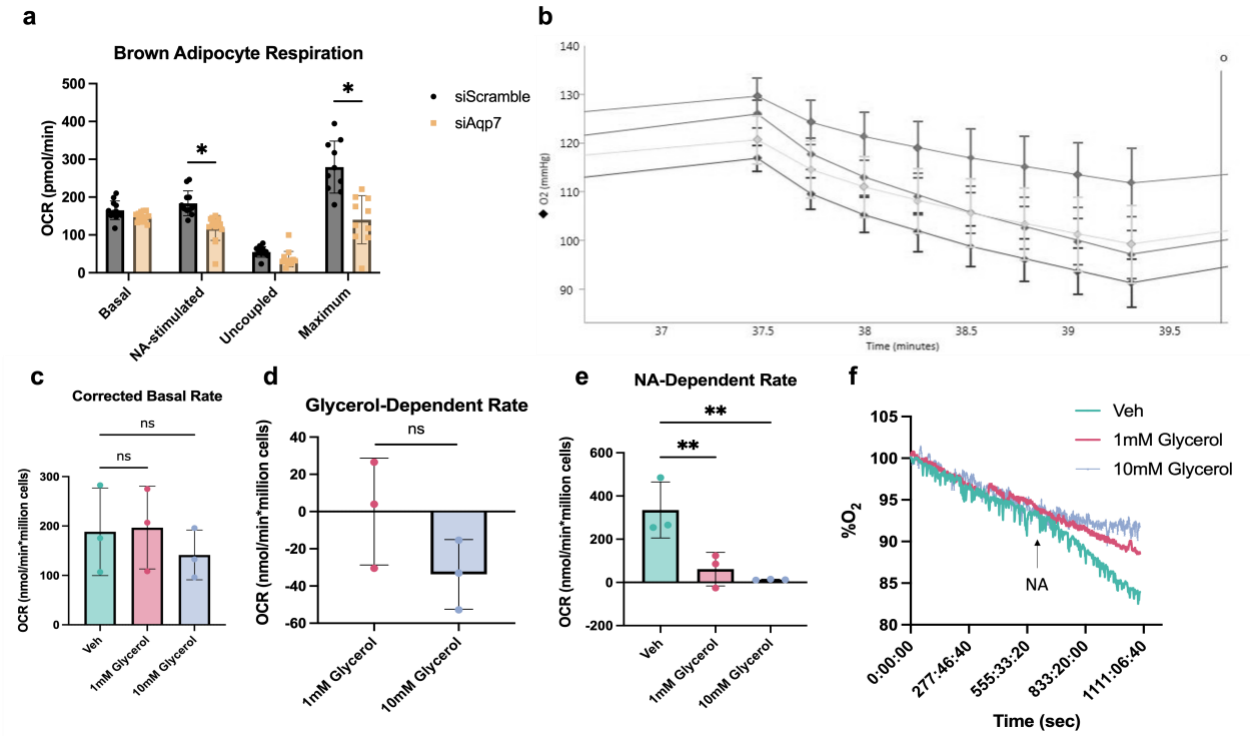

FIGURE 6. Noradrenaline-stimulated thermogenesis requires glycerol export. (**A**) Effect of *Aqp7* knockdown via siRNA on oxygen consumption rate (OCR) of mature brown adipocytes. Treatments to initiate different respiration states are as follows: stimulated, noradrenaline; uncoupled, oligomycin; maximum, 2,4-Dinitrophenol. siAqp7 treatment is a pool of four independent siRNAs (n=11-15 per group). (**B**) OCR measurement cycle in Seahorse Bioanalyzer during NA-stimulated respiration. (**C**) Basal respiration rates of freshly isolated mature brown adipocytes in the absence or presence of glycerol. (**D**) Basal respiration rates of freshly isolated mature brown adipocytes before adding glycerol (n=3 per group). (**D**) Effect of glycerol on basal respiration rates of freshly isolated mature brown adipocytes (n=3 per group). (**E**) NA-stimulated OCR above basal of freshly isolated mature brown adipocytes in the absence or presence of glycerol (n=3 per group). (**F**) Representative OCR traces indicating basal respiration rates and NA-stimulated oxygen consumption traces of freshly isolated mature brown adipocytes. (**A & D**) Unpaired student's two-tailed t-test; (**C & E**) One-way ANOVA (Fisher's LSD).

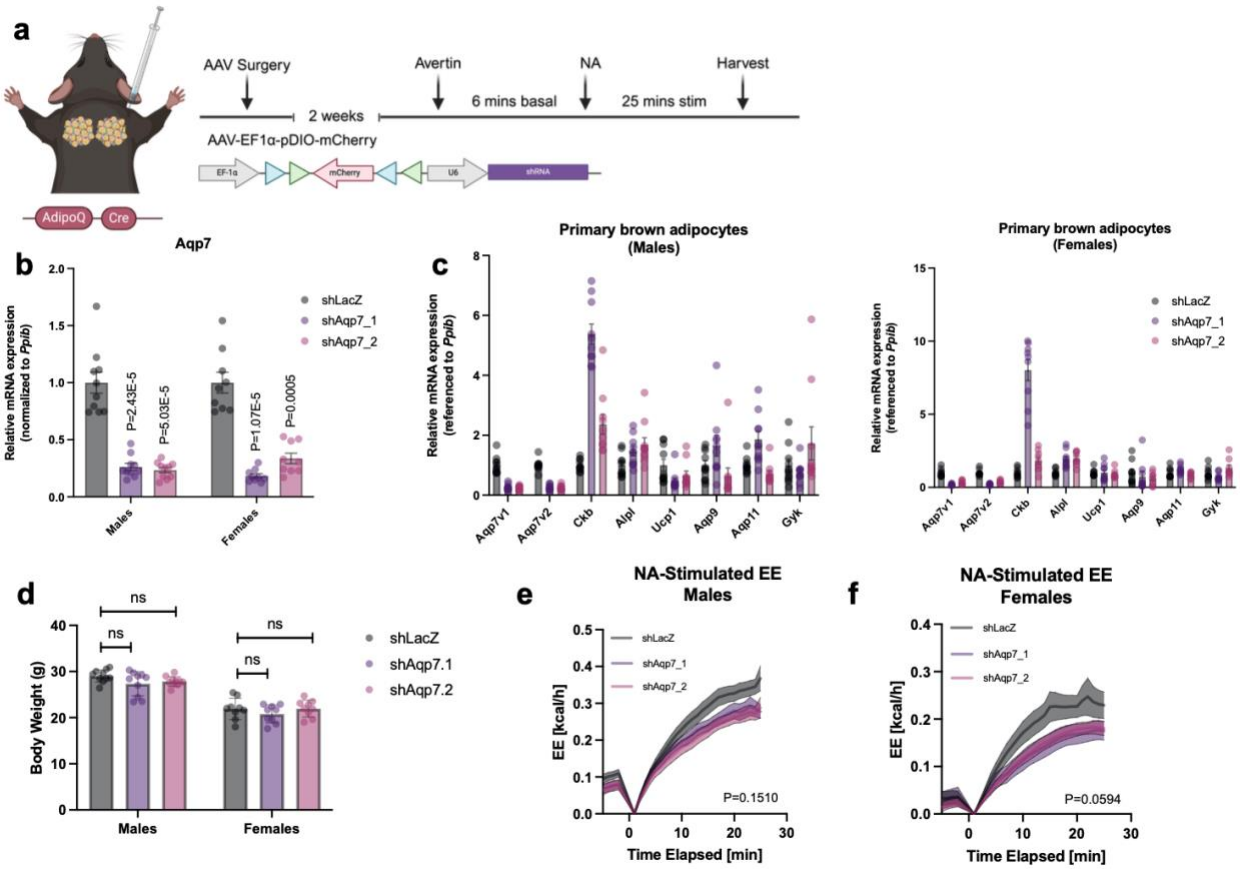

FIGURE 7. Fat-specific Aqp7 knockdown decreases whole-body energy expenditure. (**A**) Schematic of surgical delivery of AAV into intrascapular BAT depots (iBAT) of Adiponectin-Cre mice and recovery timeline before NA-stimulated energy expenditure was determined using indirect calorimetry. Created with BioRender.com (**B**) RT-qPCR of Aqp7 expression in male and female iBAT depots two weeks after AAV delivery (n=10, males; n=9, females). (**C**) RT-qPCR of male and female iBAT depots two weeks after AAV delivery (n=10, males; n=9, females). (**D**) Weight-matched post-operative mice before indirect calorimetry (n=10, males; n=10, females). (**E**) Noradrenaline-stimulated energy expenditure in post-operative male mice acclimated to RT (n=8-10 per group). (**F**) Noradrenaline-stimulated energy expenditure in post-operative female mice acclimated to RT (n=9-10 per group). Avertin-induced anesthesia from -5 to 0 min (time elapsed), NA subcutaneous injection delivered at 0 min, and NA-stimulated response observed for 25 mins. (**B-D**) One-way ANOVA (Fisher's least significant difference); (**E-F**) Two-way ANOVA (Fisher's LSD).

REFERENCES

1. Mahase, E. Global cost of overweight and obesity will hit $4.32tn a year by 2035, report warns. *Bmj* **380**, 523, doi:10.1136/bmj.p523 (2023).
2. Becher, T. *et al.* Brown adipose tissue is associated with cardiometabolic health. *Nat Med* **27**, 58-65, doi:10.1038/s41591-020-1126-7 (2021).
3. Fedorenko, A., Lishko, P. V. & Kirichok, Y. Mechanism of fatty-acid-dependent UCP1 uncoupling in brown fat mitochondria. *Cell* **151**, 400-413, doi:10.1016/j.cell.2012.09.010 (2012).
4. Kazak, L. *et al.* A creatine-driven substrate cycle enhances energy expenditure and thermogenesis in beige fat. *Cell* **163**, 643-655, doi:10.1016/j.cell.2015.09.035 (2015).
5. Mottillo, E. P. *et al.* Coupling of lipolysis and de novo lipogenesis in brown, beige, and white adipose tissues during chronic β3-adrenergic receptor activation. *J Lipid Res* **55**, 2276-2286, doi:10.1194/jlr.M050005 (2014).
6. Ukropec, J., Anunciado, R. P., Ravussin, Y., Hulver, M. W. & Kozak, L. P. UCP1-independent thermogenesis in white adipose tissue of cold-acclimated Ucp1-/- mice. *J Biol Chem* **281**, 31894-31908, doi:10.1074/jbc.M606114200 (2006).
7. Kazak, L. & Cohen, P. Creatine metabolism: energy homeostasis, immunity and cancer biology. *Nat Rev Endocrinol* **16**, 421-436, doi:10.1038/s41574-020-0365-5 (2020).
8. Rahbani, J. F. *et al.* Creatine kinase B controls futile creatine cycling in thermogenic fat. *Nature* **590**, 480-485, doi:10.1038/s41586-021-03221-y (2021).
9. Sun, Y. *et al.* Mitochondrial TNAP controls thermogenesis by hydrolysis of phosphocreatine. *Nature* **593**, 580-585, doi:10.1038/s41586-021-03533-z (2021).
10. Schreiber, R. *et al.* Cold-Induced Thermogenesis Depends on ATGL-Mediated Lipolysis in Cardiac Muscle, but Not Brown Adipose Tissue. *Cell Metab* **26**, 753-763.e757, doi:10.1016/j.cmet.2017.09.004 (2017).
11. Hibuse, T., Maeda, N., Nagasawa, A. & Funahashi, T. Aquaporins and glycerol metabolism. *Biochim Biophys Acta* **1758**, 1004-1011, doi:10.1016/j.bbamem.2006.01.008 (2006).
12. Grundy, S. M. Multifactorial causation of obesity: implications for prevention. *Am J Clin Nutr* **67**, 563s-572s, doi:10.1093/ajcn/67.3.563S (1998).
13. Eknoyan, G. Adolphe Quetelet (1796-1874)--the average man and indices of obesity. *Nephrol Dial Transplant* **23**, 47-51, doi:10.1093/ndt/gfm517 (2008).
14. Global burden of 87 risk factors in 204 countries and territories, 1990-2019: a systematic analysis for the Global Burden of Disease Study 2019. *Lancet* **396**, 1223-1249, doi:10.1016/s0140-6736(20)30752-2 (2020).
15. Worldwide trends in underweight and obesity from 1990 to 2022: a pooled analysis of 3663 population-representative studies with 222 million children, adolescents, and adults. *Lancet* **403**, 1027-1050, doi:10.1016/s0140-6736(23)02750-2 (2024).
16. Simmonds, M., Llewellyn, A., Owen, C. G. & Woolacott, N. Predicting adult obesity from childhood obesity: a systematic review and meta-analysis. *Obes Rev* **17**, 95-107, doi:10.1111/obr.12334 (2016).

17. Bancej, C. *et al.* Evidence Brief--Trends and projections of obesity among Canadians. *Health Promot Chronic Dis Prev Can* **35**, 109-112, doi:10.24095/hpcdp.35.7.02 (2015).
18. Masters, W. A., Martinez, E. M., Greb, F., Herforth, A. & Hendriks, S. L. in *Science and Innovations for Food Systems Transformation* (eds J. von Braun, K. Afsana, L. O. Fresco, & M. H. A. Hassan) 603-623 (Springer Copyright 2023, The Author(s). 2023).
19. Gulliford, M. C. *et al.* in *Costs and outcomes of increasing access to bariatric surgery for obesity: cohort study and cost-effectiveness analysis using electronic health records* (NIHR Journals Library Copyright © Queen's Printer and Controller of HMSO 2016. This work was produced by Gulliford et al. under the terms of a commissioning contract issued by the Secretary of State for Health. This issue may be freely reproduced for the purposes of private research and study and extracts (or indeed, the full report) may be included in professional journals provided that suitable acknowledgement is made and the reproduction is not associated with any form of advertising. Applications for commercial reproduction should be addressed to: NIHR Journals Library, National Institute for Health Research, Evaluation, Trials and Studies Coordinating Centre, Alpha House, University of Southampton Science Park, Southampton SO16 7NS, UK., 2016).
20. Klein, S. *et al.* Absence of an effect of liposuction on insulin action and risk factors for coronary heart disease. *N Engl J Med* **350**, 2549-2557, doi:10.1056/NEJMoa033179 (2004).
21. Atlas, S. J. *et al.* Medications for obesity management: Effectiveness and value. *J Manag Care Spec Pharm* **29**, 569-575, doi:10.18553/jmcp.2023.29.5.569 (2023).
22. Lange, J. & Königsrainer, A. Malnutrition as a Complication of Bariatric Surgery - A Clear and Present Danger? *Visc Med* **35**, 305-311, doi:10.1159/000503040 (2019).
23. Kwok, K. H., Lam, K. S. & Xu, A. Heterogeneity of white adipose tissue: molecular basis and clinical implications. *Exp Mol Med* **48**, e215, doi:10.1038/emm.2016.5 (2016).
24. Zou, M. L., Moughan, P. J., Awati, A. & Livesey, G. Accuracy of the Atwater factors and related food energy conversion factors with low-fat, high-fiber diets when energy intake is reduced spontaneously. *Am J Clin Nutr* **86**, 1649-1656, doi:10.1093/ajcn/86.5.1649 (2007).
25. Neeland, I. J. *et al.* Visceral and ectopic fat, atherosclerosis, and cardiometabolic disease: a position statement. *Lancet Diabetes Endocrinol* **7**, 715-725, doi:10.1016/s2213-8587(19)30084-1 (2019).
26. Trayhurn, P. & Beattie, J. H. Physiological role of adipose tissue: white adipose tissue as an endocrine and secretory organ. *Proc Nutr Soc* **60**, 329-339, doi:10.1079/pns200194 (2001).
27. Wang, Q. A., Tao, C., Gupta, R. K. & Scherer, P. E. Tracking adipogenesis during white adipose tissue development, expansion and regeneration. *Nature Medicine* **19**, 1338-1344, doi:10.1038/nm.3324 (2013).

28. Shan, T. *et al.* Distinct populations of adipogenic and myogenic Myf5-lineage progenitors in white adipose tissues. *J Lipid Res* **54**, 2214-2224, doi:10.1194/jlr.M038711 (2013).
29. Konige, M., Wang, H. & Sztalryd, C. Role of adipose specific lipid droplet proteins in maintaining whole body energy homeostasis. *Biochim Biophys Acta* **1842**, 393-401, doi:10.1016/j.bbadis.2013.05.007 (2014).
30. Longo, M. *et al.* Adipose Tissue Dysfunction as Determinant of Obesity-Associated Metabolic Complications. *Int J Mol Sci* **20**, doi:10.3390/ijms20092358 (2019).
31. Rowland, L. A. *et al.* De novo lipogenesis fuels adipocyte autophagosome and lysosome membrane dynamics. *Nature Communications* **14**, 1362, doi:10.1038/s41467-023-37016-8 (2023).
32. Chitraju, C., Walther, T. C. & Farese, R. V. The triglyceride synthesis enzymes DGAT1 and DGAT2 have distinct and overlapping functions in adipocytes. *Journal of Lipid Research* **60**, 1112-1120, doi:10.1194/jlr.M093112 (2019).
33. Krotkiewski, M., Björntorp, P., Sjöström, L. & Smith, U. Impact of obesity on metabolism in men and women. Importance of regional adipose tissue distribution. *J Clin Invest* **72**, 1150-1162, doi:10.1172/jci111040 (1983).
34. Spalding, K. L. *et al.* Dynamics of fat cell turnover in humans. *Nature* **453**, 783-787, doi:10.1038/nature06902 (2008).
35. Achilike, I., Hazuda, H. P., Fowler, S. P., Aung, K. & Lorenzo, C. Predicting the development of the metabolically healthy obese phenotype. *Int J Obes (Lond)* **39**, 228-234, doi:10.1038/ijo.2014.113 (2015).
36. Yazıcı, D. & Sezer, H. Insulin Resistance, Obesity and Lipotoxicity. *Adv Exp Med Biol* **960**, 277-304, doi:10.1007/978-3-319-48382-5_12 (2017).
37. Cinti, S. *et al.* Adipocyte death defines macrophage localization and function in adipose tissue of obese mice and humans. *J Lipid Res* **46**, 2347-2355, doi:10.1194/jlr.M500294-JLR200 (2005).
38. Rodgers, J. T. & Puigserver, P. Fasting-dependent glucose and lipid metabolic response through hepatic sirtuin 1. *Proceedings of the National Academy of Sciences* **104**, 12861-12866, doi:doi:10.1073/pnas.0702509104 (2007).
39. Young, S. G. & Zechner, R. Biochemistry and pathophysiology of intravascular and intracellular lipolysis. *Genes Dev* **27**, 459-484, doi:10.1101/gad.209296.112 (2013).
40. Recazens, E., Mouisel, E. & Langin, D. Hormone-sensitive lipase: sixty years later. *Prog Lipid Res* **82**, 101084, doi:10.1016/j.plipres.2020.101084 (2021).
41. Al-Mass, A. *et al.* Hepatic glycerol shunt and glycerol-3-phosphate phosphatase control liver metabolism and glucodetoxification under hyperglycemia. *Mol Metab* **66**, 101609, doi:10.1016/j.molmet.2022.101609 (2022).
42. Hopkin, M. Fat cell numbers stay constant through adult life. *Nature*, doi:10.1038/news.2008.800 (2008).
43. Löfgren, P. *et al.* Long-term prospective and controlled studies demonstrate adipose tissue hypercellularity and relative leptin deficiency in the postobese state. *J Clin Endocrinol Metab* **90**, 6207-6213, doi:10.1210/jc.2005-0596 (2005).
44. Gessner, C., Rondelet, G., Belon, P. & Froschauer, C. *Conradi Gesneri ... Historiae animalium lib. I[-IIII]*. (apvd Christ. Froschoverum, 1551).

45. Chaffee, R. R. J. *et al.* Studies on thermogenesis in brown adipose tissue in temperature-acclimated Macaca mulatta. *Comparative Biochemistry and Physiology Part A: Physiology* **50**, 303-306, doi:https://doi.org/10.1016/0300-9629(75)90017-1 (1975).
46. Foster, D. O. & Frydman, M. L. Nonshivering thermogenesis in the rat. II. Measurements of blood flow with microspheres point to brown adipose tissue as the dominant site of the calorigenesis induced by noradrenaline. *Can J Physiol Pharmacol* **56**, 110-122, doi:10.1139/y78-015 (1978).
47. Foster, D. O. & Frydman, M. L. Tissue distribution of cold-induced thermogenesis in conscious warm- or cold-acclimated rats reevaluated from changes in tissue blood flow: the dominant role of brown adipose tissue in the replacement of shivering by nonshivering thermogenesis. *Can J Physiol Pharmacol* **57**, 257-270, doi:10.1139/y79- 039 (1979).
48. Foster, D. O. & Frydman, M. L. Nonshivering thermogenesis in the rat. II. Measurements of blood flow with microspheres point to brown adipose tissue as the dominant site of the calorigenesis induced by noradrenaline. *Canadian Journal of Physiology and Pharmacology* **56**, 110-122, doi:10.1139/y78-015 (1978).
49. Foster, D. O. & Frydman, M. L. Tissue distribution of cold-induced thermogenesis in conscious warm- or cold-acclimated rats reevaluated from changes in tissue blood flow: The dominant role of brown adipose tissue in the replacement of shivering by nonshivering thermogenesis. *Canadian Journal of Physiology and Pharmacology* **57**, 257-270, doi:10.1139/y79-039 (1979).
50. Urisarri, A. *et al.* BMP8 and activated brown adipose tissue in human newborns. *Nat Commun* **12**, 5274, doi:10.1038/s41467-021-25456-z (2021).
51. Cypess, A. M. *et al.* Identification and Importance of Brown Adipose Tissue in Adult Humans. *New England Journal of Medicine* **360**, 1509-1517, doi:doi:10.1056/NEJMoa0810780 (2009).
52. Virtanen, K. A. *et al.* Functional Brown Adipose Tissue in Healthy Adults. *New England Journal of Medicine* **360**, 1518-1525, doi:doi:10.1056/NEJMoa0808949 (2009).
53. Saito, M. *et al.* High Incidence of Metabolically Active Brown Adipose Tissue in Healthy Adult Humans: Effects of Cold Exposure and Adiposity. *Diabetes* **58**, 1526-1531, doi:10.2337/db09-0530 (2009).
54. Rothwell, N. J. & Stock, M. J. A role for brown adipose tissue in diet-induced thermogenesis. *Nature* **281**, 31-35, doi:10.1038/281031a0 (1979).
55. Trayhurn, P., Thurlby, P. L. & James, W. P. Thermogenic defect in pre-obese ob/ob mice. *Nature* **266**, 60-62, doi:10.1038/266060a0 (1977).
56. Aita, S. *et al.* Brown fat-associated postprandial thermogenesis in humans: Different effects of isocaloric meals rich in carbohydrate, fat, and protein. *Front Nutr* **9**, 1040444, doi:10.3389/fnut.2022.1040444 (2022).
57. Seale, P. *et al.* PRDM16 controls a brown fat/skeletal muscle switch. *Nature* **454**, 961-967, doi:10.1038/nature07182 (2008).
58. Lepper, C. & Fan, C. M. Inducible lineage tracing of Pax7-descendant cells reveals embryonic origin of adult satellite cells. *Genesis* **48**, 424-436, doi:10.1002/dvg.20630 (2010).

59. Rajakumari, S. *et al.* EBF2 determines and maintains brown adipocyte identity. *Cell Metab* **17**, 562-574, doi:10.1016/j.cmet.2013.01.015 (2013).
60. Christodoulides, C., Lagathu, C., Sethi, J. K. & Vidal-Puig, A. Adipogenesis and WNT signalling. *Trends Endocrinol Metab* **20**, 16-24, doi:10.1016/j.tem.2008.09.002 (2009).
61. Engel, B. T., Sato, A. & Sato, Y. Responses of sympathetic nerves innervating blood vessels in interscapular, brown adipose tissue and skin during cold stimulation in anesthetized C57BL/6J mice. *Jpn J Physiol* **42**, 549-559, doi:10.2170/jjphysiol.42.549 (1992).
62. Wirsen, C. Adrenergic Innervation of Adipose Tissue Examined by Fluorescence Microscopy. *Nature* **202**, 913, doi:10.1038/202913a0 (1964).
63. Cottle, W. H., Nash, C. W., Veress, A. T. & Ferguson, B. A. Release of noradrenaline from fat of cold-acclimated rats. *Life Sci* **6**, 2267-2271, doi:10.1016/0024- 3205(67)90034-3 (1967).
64. Horwitz, B. A., Horowitz, J. M., Jr. & Smith, R. E. Norepinephrine-induced depolarization of brown fat cells. *Proc Natl Acad Sci U S A* **64**, 113-120, doi:10.1073/pnas.64.1.113 (1969).
65. Geslot, A. *et al.* Weight-loss with activation of brown fat: Suspect pheochromocytoma. *Ann Endocrinol (Paris)* **80**, 314-318, doi:10.1016/j.ando.2019.06.004 (2019).
66. Minneman, K. P., Theroux, T. L., Hollinger, S., Han, C. & Esbenshade, T. A. Selectivity of agonists for cloned alpha 1-adrenergic receptor subtypes. *Mol Pharmacol* **46**, 929-936 (1994).
67. Muzzin, P. *et al.* An adipose tissue-specific beta-adrenergic receptor. Molecular cloning and down-regulation in obesity. *J Biol Chem* **266**, 24053-24058 (1991).
68. Krintel, C., Mörgelin, M., Logan, D. T. & Holm, C. Phosphorylation of hormone-sensitive lipase by protein kinase A in vitro promotes an increase in its hydrophobic surface area. *Febs j* **276**, 4752-4762, doi:10.1111/j.1742-4658.2009.07172.x (2009).
69. Houten, S. M. & Wanders, R. J. A general introduction to the biochemistry of mitochondrial fatty acid β-oxidation. *J Inherit Metab Dis* **33**, 469-477, doi:10.1007/s10545-010-9061-2 (2010).
70. Gonzalez, G. A. & Montminy, M. R. Cyclic AMP stimulates somatostatin gene transcription by phosphorylation of CREB at serine 133. *Cell* **59**, 675-680, doi:10.1016/0092-8674(89)90013-5 (1989).
71. Yamamoto, K. K., Gonzalez, G. A., Biggs, W. H., 3rd & Montminy, M. R. Phosphorylation-induced binding and transcriptional efficacy of nuclear factor CREB. *Nature* **334**, 494-498, doi:10.1038/334494a0 (1988).
72. Herzig, S. *et al.* CREB regulates hepatic gluconeogenesis through the coactivator PGC-1. *Nature* **413**, 179-183, doi:10.1038/35093131 (2001).
73. Puigserver, P. *et al.* A cold-inducible coactivator of nuclear receptors linked to adaptive thermogenesis. *Cell* **92**, 829-839, doi:10.1016/s0092-8674(00)81410-5 (1998).
74. Wu, Z. *et al.* Mechanisms controlling mitochondrial biogenesis and respiration through the thermogenic coactivator PGC-1. *Cell* **98**, 115-124, doi:10.1016/S0092- 8674(00)80611-X (1999).

75. Rohas, L. M. *et al.* A fundamental system of cellular energy homeostasis regulated by PGC-1alpha. *Proc Natl Acad Sci U S A* **104**, 7933-7938, doi:10.1073/pnas.0702683104 (2007).
76. Brown, E. L. *et al.* Estrogen-Related Receptors Mediate the Adaptive Response of Brown Adipose Tissue to Adrenergic Stimulation. *iScience* **2**, 221-237, doi:10.1016/j.isci.2018.03.005 (2018).
77. Fink, S. A. & Williams, J. A. Adrenergic receptors mediating depolarization in brown adipose tissue. *Am J Physiol* **231**, 700-706, doi:10.1152/ajplegacy.1976.231.3.700 (1976).
78. Klepac, K. *et al.* The Gq signalling pathway inhibits brown and beige adipose tissue. *Nature Communications* **7**, 10895, doi:10.1038/ncomms10895 (2016).
79. Schmitz, E. A., Takahashi, H. & Karakas, E. Structural basis for activation and gating of IP3 receptors. *Nature Communications* **13**, 1408, doi:10.1038/s41467-022-29073-2 (2022).
80. Ventura, C. & Maioli, M. Protein kinase C control of gene expression. *Crit Rev Eukaryot Gene Expr* **11**, 243-267 (2001).
81. Robidoux, J., Martin, T. L. & Collins, S. Beta-adrenergic receptors and regulation of energy expenditure: a family affair. *Annu Rev Pharmacol Toxicol* **44**, 297-323, doi:10.1146/annurev.pharmtox.44.101802.121659 (2004).
82. Rahbani, J. F. *et al.* ADRA1A-Gα(q) signalling potentiates adipocyte thermogenesis through CKB and TNAP. *Nat Metab* **4**, 1459-1473, doi:10.1038/s42255-022-00667-w (2022).
83. Oguri, Y. & Kajimura, S. Cellular heterogeneity in brown adipose tissue. *The Journal of Clinical Investigation* **130**, 65-67, doi:10.1172/JCI133786 (2020).
84. Grundlingh, J., Dargan, P. I., El-Zanfaly, M. & Wood, D. M. 2,4-dinitrophenol (DNP): a weight loss agent with significant acute toxicity and risk of death. *J Med Toxicol* **7**, 205-212, doi:10.1007/s13181-011-0162-6 (2011).
85. Nicholls, D. G. & Rial, E. A history of the first uncoupling protein, UCP1. *J Bioenerg Biomembr* **31**, 399-406, doi:10.1023/a:1005436121005 (1999).
86. Heaton, G. M., Wagenvoord, R. J., Kemp, A., Jr. & Nicholls, D. G. Brown-adipose-tissue mitochondria: photoaffinity labelling of the regulatory site of energy dissipation. *Eur J Biochem* **82**, 515-521, doi:10.1111/j.1432-1033.1978.tb12045.x (1978).
87. Klingenberg, M. & Winkler, E. The reconstituted isolated uncoupling protein is a membrane potential driven H+ translocator. *EMBO J* **4**, 3087-3092 (1985).
88. Rafael, J. & Heldt, H. W. Binding of guanine nucleotides to the outer surface of the inner membrane of guinea pig brown fat mitochondria in correlation with the thermogenic activity of the tissue. *FEBS Lett* **63**, 304-308, doi:10.1016/0014-5793(76)80117-2 (1976).
89. Shabalina, I. G., Jacobsson, A., Cannon, B. & Nedergaard, J. Native UCP1 displays simple competitive kinetics between the regulators purine nucleotides and fatty acids. *J Biol Chem* **279**, 38236-38248, doi:10.1074/jbc.M402375200 (2004).
90. Jones, S. A. *et al.* Structural basis of purine nucleotide inhibition of human uncoupling protein 1. *Science Advances* **9**, eadh4251, doi:doi:10.1126/sciadv.adh4251 (2023).

91. Villarroya, F., Peyrou, M. & Giralt, M. Transcriptional regulation of the uncoupling protein-1 gene. *Biochimie* **134**, 86-92, doi:10.1016/j.biochi.2016.09.017 (2017).
92. Golozoubova, V. *et al.* Only UCP1 can mediate adaptive nonshivering thermogenesis in the cold. *FASEB J* **15**, 2048-2050, doi:10.1096/fj.00-0536fje (2001).
93. Liu, X. *et al.* Paradoxical resistance to diet-induced obesity in UCP1-deficient mice. *J Clin Invest* **111**, 399-407, doi:10.1172/JCI15737 (2003).
94. Hofmann, W. E., Liu, X., Bearden, C. M., Harper, M. E. & Kozak, L. P. Effects of genetic background on thermoregulation and fatty acid-induced uncoupling of mitochondria in UCP1-deficient mice. *J Biol Chem* **276**, 12460-12465, doi:10.1074/jbc.M100466200 (2001).
95. Kazak, L. *et al.* UCP1 deficiency causes brown fat respiratory chain depletion and sensitizes mitochondria to calcium overload-induced dysfunction. *Proc Natl Acad Sci U S A* **114**, 7981-7986, doi:10.1073/pnas.1705406114 (2017).
96. Rahbani, J. F. *et al.* Parallel control of cold-triggered adipocyte thermogenesis by UCP1 and CKB. *Cell Metab* **36**, 526-540.e527, doi:10.1016/j.cmet.2024.01.001 (2024).
97. Enerback, S. *et al.* Mice lacking mitochondrial uncoupling protein are cold-sensitive but not obese. *Nature* **387**, 90-94, doi:10.1038/387090a0 (1997).
98. Oeckl, J. *et al.* Loss of UCP1 function augments recruitment of futile lipid cycling for thermogenesis in murine brown fat. *Mol Metab* **61**, 101499, doi:10.1016/j.molmet.2022.101499 (2022).
99. Kazak, L. *et al.* Ablation of adipocyte creatine transport impairs thermogenesis and causes diet-induced obesity. *Nat Metab* **1**, 360-370, doi:10.1038/s42255-019-0035-x (2019).
100. Kazak, L. *et al.* Genetic Depletion of Adipocyte Creatine Metabolism Inhibits Diet-Induced Thermogenesis and Drives Obesity. *Cell Metab* **26**, 660-671.e663, doi:10.1016/j.cmet.2017.08.009 (2017).
101. Ikeda, K. *et al.* UCP1-independent signaling involving SERCA2b-mediated calcium cycling regulates beige fat thermogenesis and systemic glucose homeostasis. *Nat Med* **23**, 1454-1465, doi:10.1038/nm.4429 (2017).
102. Jacobus, W. E. & Lehninger, A. L. Creatine kinase of rat heart mitochondria. Coupling of creatine phosphorylation to electron transport. *J Biol Chem* **248**, 4803-4810 (1973).
103. Berlet, H. H., Bonsmann, I. & Birringer, H. Occurrence of free creatine, phosphocreatine and creatine phosphokinase in adipose tissue. *Biochimica et Biophysica Acta (BBA) - General Subjects* **437**, 166-174, doi:https://doi.org/10.1016/0304-4165(76)90358-5 (1976).
104. Wakatsuki, T. *et al.* Thermogenic responses to high-energy phosphate contents and/or hindlimb suspension in rats. *Jpn J Physiol* **46**, 171-175, doi:10.2170/jjphysiol.46.171 (1996).
105. Yamashita, H. *et al.* Increased growth of brown adipose tissue but its reduced thermogenic activity in creatine-depleted rats fed beta-guanidinopropionic acid. *Biochim Biophys Acta* **1230**, 69-73, doi:10.1016/0005-2728(95)00067-s (1995).

106. Bertholet, A. M. *et al.* Mitochondrial Patch Clamp of Beige Adipocytes Reveals UCP1-Positive and UCP1-Negative Cells Both Exhibiting Futile Creatine Cycling. *Cell Metab* **25**, 811-822.e814, doi:10.1016/j.cmet.2017.03.002 (2017).
107. Kazak, L. *et al.* Genetic Depletion of Adipocyte Creatine Metabolism Inhibits Diet-Induced Thermogenesis and Drives Obesity. *Cell Metab* **26**, 660-671.e663, doi:10.1016/j.cmet.2017.08.009 (2017).
108. Kazak, L. *et al.* Ablation of adipocyte creatine transport impairs thermogenesis and causes diet-induced obesity. *Nat Metab* **1**, 360-370, doi:10.1038/s42255-019-0035-x (2019).
109. Eliuk, S. M., Renfrow, M. B., Shonsey, E. M., Barnes, S. & Kim, H. active site modifications of the brain isoform of creatine kinase by 4-hydroxy-2-nonenal correlate with reduced enzyme activity: mapping of modified sites by Fourier transform-ion cyclotron resonance mass spectrometry. *Chem Res Toxicol* **20**, 1260-1268, doi:10.1021/tx7000948 (2007).
110. Sergienko, E. *et al.* Identification and characterization of novel tissue-nonspecific alkaline phosphatase inhibitors with diverse modes of action. *J Biomol Screen* **14**, 824-837, doi:10.1177/1087057109338517 (2009).
111. Agre, P. *et al.* Aquaporin CHIP: the archetypal molecular water channel. *Am J Physiol* **265**, F463-476, doi:10.1152/ajprenal.1993.265.4.F463 (1993).
112. Roudier, N., Verbavatz, J. M., Maurel, C., Ripoche, P. & Tacnet, F. Evidence for the presence of aquaporin-3 in human red blood cells. *J Biol Chem* **273**, 8407-8412, doi:10.1074/jbc.273.14.8407 (1998).
113. Tradtrantip, L., Jin, B. J., Yao, X., Anderson, M. O. & Verkman, A. S. Aquaporin-Targeted Therapeutics: State-of-the-Field. *Adv Exp Med Biol* **969**, 239-250, doi:10.1007/978-94-024-1057-0_16 (2017).
114. Abir-Awan, M. *et al.* Inhibitors of Mammalian Aquaporin Water Channels. *Int J Mol Sci* **20**, doi:10.3390/ijms20071589 (2019).
115. Yool, A. J. & Weinstein, A. M. New roles for old holes: ion channel function in aquaporin-1. *News Physiol Sci* **17**, 68-72, doi:10.1152/nips.01372.2001 (2002).
116. Eriksson, U. K. *et al.* Subangstrom resolution X-ray structure details aquaporin-water interactions. *Science* **340**, 1346-1349, doi:10.1126/science.1234306 (2013).
117. Nielsen, S., Smith, B. L., Christensen, E. I. & Agre, P. Distribution of the aquaporin CHIP in secretory and resorptive epithelia and capillary endothelia. *Proc Natl Acad Sci U S A* **90**, 7275-7279, doi:10.1073/pnas.90.15.7275 (1993).
118. Simone, L. *et al.* Aquaporin-1 inhibition reduces metastatic formation in a mouse model of melanoma. *J Cell Mol Med* **22**, 904-912, doi:10.1111/jcmm.13378 (2018).
119. Hara-Chikuma, M. *et al.* Progressive adipocyte hypertrophy in aquaporin-7-deficient mice: adipocyte glycerol permeability as a novel regulator of fat accumulation. *J Biol Chem* **280**, 15493-15496, doi:10.1074/jbc.C500028200 (2005).
120. Maeda, N., Hibuse, T. & Funahashi, T. Role of aquaporin-7 and aquaporin-9 in glycerol metabolism; involvement in obesity. *Handb Exp Pharmacol*, 233-249, doi:10.1007/978-3-540-79885-9_12 (2009).

121. Hibuse, T. *et al.* Aquaporin 7 deficiency is associated with development of obesity through activation of adipose glycerol kinase. *Proc Natl Acad Sci U S A* **102**, 10993-10998, doi:10.1073/pnas.0503291102 (2005).
122. Maeda, N. *et al.* Adaptation to fasting by glycerol transport through aquaporin 7 in adipose tissue. *Proc Natl Acad Sci U S A* **101**, 17801-17806, doi:10.1073/pnas.0406230101 (2004).
123. Chua, R. & Ghosh, S. An optimized method for gene knockdown in differentiating human and mouse adipocyte cultures. *bioRxiv*, doi:10.1101/2023.12.14.571780 (2023).
124. Isidor, M. S. *et al.* An siRNA-based method for efficient silencing of gene expression in mature brown adipocytes. *Adipocyte* **5**, 175-185, doi:10.1080/21623945.2015.1111972 (2016).
125. Oeckl, J., Bast-Habersbrunner, A., Fromme, T., Klingenspor, M. & Li, Y. Isolation, Culture, and Functional Analysis of Murine Thermogenic Adipocytes. *STAR Protoc* **1**, 100118, doi:10.1016/j.xpro.2020.100118 (2020).
126. Sanjana, N. E., Shalem, O. & Zhang, F. Improved vectors and genome-wide libraries for CRISPR screening. *Nat Methods* **11**, 783-784, doi:10.1038/nmeth.3047 (2014).
127. Shalem, O. *et al.* Genome-scale CRISPR-Cas9 knockout screening in human cells. *Science* **343**, 84-87, doi:10.1126/science.1247005 (2014).
128. Qiu, Y. & Ding, Q. Optimized protocol for gene editing in adipocytes using CRISPR-Cas9 technology. *STAR Protoc* **2**, 100307, doi:10.1016/j.xpro.2021.100307 (2021).
129. Larcombe, M. R. *et al.* Production of High-Titer Lentiviral Particles for Stable Genetic Modification of Mammalian Cells. *Methods Mol Biol* **1940**, 47-61, doi:10.1007/978-1-4939-9086-3_4 (2019).
130. Favuzzi, E. *et al.* Distinct molecular programs regulate synapse specificity in cortical inhibitory circuits. *Science* **363**, 413-417, doi:10.1126/science.aau8977 (2019).
131. Huang, W., Queen, N. J. & Cao, L. rAAV-Mediated Gene Delivery to Adipose Tissue. *Methods Mol Biol* **1950**, 389-405, doi:10.1007/978-1-4939-9139-6_23 (2019).
132. Long, J. Z. *et al.* A smooth muscle-like origin for beige adipocytes. *Cell Metab* **19**, 810-820, doi:10.1016/j.cmet.2014.03.025 (2014).
133. Kong, X., Williams, K. W. & Liu, T. Genetic Mouse Models: The Powerful Tools to Study Fat Tissues. *Methods Mol Biol* **1566**, 99-107, doi:10.1007/978-1-4939-6820-6_10 (2017).
134. Chu, D. T., Malinowska, E., Gawronska-Kozak, B. & Kozak, L. P. Expression of adipocyte biomarkers in a primary cell culture models reflects preweaning adipobiology. *J Biol Chem* **289**, 18478-18488, doi:10.1074/jbc.M114.555821 (2014).
135. Puigserver, P. *et al.* A cold-inducible coactivator of nuclear receptors linked to adaptive thermogenesis. *Cell* **92**, 829-839, doi:10.1016/s0092-8674(00)81410-5 (1998).

136. Brown, E. L. *et al.* Estrogen-Related Receptors Mediate the Adaptive Response of Brown Adipose Tissue to Adrenergic Stimulation. *iScience* **2**, 221-237, doi:10.1016/j.isci.2018.03.005 (2018).
137. Angueira, A. R. *et al.* Early B Cell Factor Activity Controls Developmental and Adaptive Thermogenic Gene Programming in Adipocytes. *Cell Rep* **30**, 2869-2878.e2864, doi:10.1016/j.celrep.2020.02.023 (2020).
138. Kilroy, G., Burk, D. H. & Floyd, Z. E. High efficiency lipid-based siRNA transfection of adipocytes in suspension. *PLoS One* **4**, e6940, doi:10.1371/journal.pone.0006940 (2009).
139. Sonntag, Y. *et al.* Identification and characterization of potent and selective aquaporin-3 and aquaporin-7 inhibitors. *J Biol Chem* **294**, 7377-7387, doi:10.1074/jbc.RA118.006083 (2019).
140. Kuhn, M., Santinha, A. J. & Platt, R. J. Moving from in vitro to in vivo CRISPR screens. *Gene and Genome Editing* **2**, 100008, doi:https://doi.org/10.1016/j.ggedit.2021.100008 (2021).
141. Gómez-García, I., Trepiana, J., Fernández-Quintela, A., Giralt, M. & Portillo, M. P. Sexual Dimorphism in Brown Adipose Tissue Activation and White Adipose Tissue Browning. *Int J Mol Sci* **23**, doi:10.3390/ijms23158250 (2022).
142. Mills, E. L. *et al.* Accumulation of succinate controls activation of adipose tissue thermogenesis. *Nature* **560**, 102-106, doi:10.1038/s41586-018-0353-2 (2018).
143. He, X. *et al.* The PI3K/AKT signalling pathway in inflammation, cell death and glial scar formation after traumatic spinal cord injury: Mechanisms and therapeutic opportunities. *Cell Prolif* **55**, e13275, doi:10.1111/cpr.13275 (2022).
144. Saito, T., Tanaka, Y., Morishita, Y. & Ishibashi, K. Proteomic analysis of AQP11-null kidney: Proximal tubular type polycystic kidney disease. *Biochem Biophys Rep* **13**, 17-21, doi:10.1016/j.bbrep.2017.11.003 (2018).
145. Gama-Norton, L. *et al.* Lentivirus production is influenced by SV40 large T-antigen and chromosomal integration of the vector in HEK293 cells. *Hum Gene Ther* **22**, 1269-1279, doi:10.1089/hum.2010.143 (2011).
146. Bryan, T. M. & Reddel, R. R. SV40-induced immortalization of human cells. *Crit Rev Oncog* **5**, 331-357, doi:10.1615/critrevoncog.v5.i4.10 (1994).
147. Engin, A. B. What Is Lipotoxicity? *Adv Exp Med Biol* **960**, 197-220, doi:10.1007/978-3-319-48382-5_8 (2017).
148. Kotzbeck, P. *et al.* Brown adipose tissue whitening leads to brown adipocyte death and adipose tissue inflammation. *J Lipid Res* **59**, 784-794, doi:10.1194/jlr.M079665 (2018).